GENERAL ATOMIC

DIVISION OF GENERAL DYNAMICS

GA-4386

EXPERIMENTAL BERYLLIUM OXIDE REACTOR PROGRAM

QUARTERLY PROGRESS REPORT

for the period ending
June 30, 1963

U.S. Atomic Energy Commission
Contract AT(04-3)-187

July 31, 1963

DISCLAIMER

GENERAL ATOMIC

DIVISION OF

GENERAL DYNAMICS

JOHN JAY HOPKINS LABORATORY FOR PURE AND APPLIED SCIENCE

P.O. BOX 608. SAN DIEGO 12. CALIFORNIA

GA-4386

EXPERIMENTAL BERYLLIUM OXIDE REACTOR PROGRAM

QUARTERLY PROGRESS REPORT

for the period ending
June 30, 1963

U.S. Atomic Energy Commission
Contract AT(04-3)-187

July 31, 1963

PREVIOUS REPORTS IN THIS SERIES

GA-2372—April, May, June, 1961

GA-2568—July, August, September, 1961

GA-2847—October, November, December, 1961

GA-3053—January, February, March, 1962

GA-3307—April, May, June, 1962 (Prelim.)

GA-3561—July, August, September, 1962 (Prelim.)

GA-3830—October, November, December, 1962 (Prelim.)

GA-4124—January, February, March, 1963

FOREWORD

The Experimental Beryllium Oxide Reactor (EBOR) Program, formerly the Maritime Gas-cooled Reactor (MGCR) Program, was initiated February 17, 1958, under Contract AT(04-3)-187 between the U.S. Atomic Energy Commission and Maritime Administration and General Dynamics Corporation. In December of 1960, formal authorization was received to reorient the program to include as an intermediate stage the design, construction, and test operation of a 10-megawatt (thermal) reactor experiment for the purpose of determining the operating characteristics of BeO-moderated, gas-cooled systems and of lending greater assurance of success to the subsequent prototype plant. This reactor experiment is known as the Experimental Beryllium Oxide Reactor.

The objective of the EBOR program is to develop a gas-cooled, BeO-moderated reactor that can be used in conjunction with a closed-cycle gas turbine or a steam cycle for a small land-based or a maritime power plant. Design objectives for the power plant are high thermodynamic efficiency, simplicity of design with attendant ease of operation, low maintenance costs, and maximum efficiency of operation over a wide range of power settings.

THIS PAGE

WAS INTENTIONALLY

LEFT BLANK

CONTENTS

I. SUMMARY

REACTOR

During the quarter, work was initiated on the design of the reactor-startup source element. A single 50-curie Po-Be source is being designed to meet the requirements of reactor startup.

Design and procurement action was initiated for the first phase of the tipping-reflector-element test program. Design of the test model and apparatus is complete and fabrication is in process.

A new series of environmental tests of fuel-pin specimens consisting of depleted 57 UO_2—43 BeO (weight percent) clad with Hastelloy-X-280 was initiated. Each of six fuel-pin specimens was clad from a separate lot of the production Hastelloy-X-280 to obtain random sampling of the production tubing.

The thermal-performance analysis of the 36-element core was completed for the case of the steady-state design point with start-of-life power generation. Under these conditions, the total power produced is 10 megawatts, 9.6 megawatts being produced in the core and 0.4 megawatt in the vessel and internal components. Results show that the mixed-mean coolant-outlet temperature from the core is 1300°F and the reactor-outlet-duct temperature is 1270°F. The over-all reactor pressure is 18.1 psi.

The pressure-vessel flow model has been fabricated and delivered. The model was subsequently checked for leaks and mounted in the test stand. A special flow meter for measuring the amount of bypass flow was installed in the flow model and is presently undergoing calibration.

CONSTRUCTION AND PROCUREMENT

Design proposals, based on the criterion of removability at site, were prepared for the coolant inlet-orifice inserts for the reflector elements.

Four pellet-fabrication trial runs have been completed to date. The fourth run was made using a single standardized process during the entire run and produced 5500 pellets from seeded UO_2 and as-received BeO.

Major steps accomplished during the quarter in the area of pressure-vessel fabrication include: (1) arrival of the pressure-vessel top-head flange and dish forgings, (2) delivery of the pressure-vessel shell flange, and (3) welding of thermal-shield course C-3 longitudinal seams using Automatic Welding Procedure WP-34.

Prototype tests of the control-rod-drive mechanism are scheduled to begin early in August, 1963.

Todd Shipyards, vendor for the modification of the Shield Test Facility (STF) instrument bridge, inspected the existing assembly at the Idaho test site preparatory to beginning work.

REACTOR PHYSICS

Reactivity calculations pertaining to completion of the nuclear-design analysis of the EBOR reference-design core were completed during the quarter. In particular, the variation of reactivity with lifetime, the radial- and axial-power distributions, and the total and differential control-rod-bank worths were re-established. Additionally, a formal report summarizing the temperature-coefficient calculations, including the effect of Doppler broadening of the U^{235} resonances, was issued.

Two special computer programs were prepared to enable contour maps of the flux, integrated flux, and power distributions to be automatically plotted using the SC-4020 plotter. The programs greatly facilitate the presentation of data on EBOR and will be used to generate curves for a final formal report on the nuclear characteristics of the reactor.

Work was initiated on the preparation of those sections of the final hazards report that require physics calculations. Combined heat-transfer and reactor-kinetics calculations were run using a modified version of the General Atomic developed code BLOOST-2. Cases involving various ramp and step reactivity insertions were completed and the results are presented herein.

MATERIALS DEVELOPMENT

The high-temperature irradiation of capsule MGCR-4 in the Materials Testing Reactor (MTR) was terminated in mid-March, after 11,700 hours of irradiation encompassing 170 temperature cycles at full power had been accumulated. This corresponds to an estimated peak burnup of 4.8 percent of the uranium atoms present (approximately 3.6×10^{20} fissions/cm^3; 42,000 Mwd/ton of uranium).

Postoperation examination of capsule MGCR-BRR-9 continued during the quarter. Density determinations for the fuel pellets revealed a linear increase of about 1.5 percent. Fine- and coarse-particle fuel pellets exhibited no differences in linear change. Fission-gas-release measurements showed that the coarse-particle fuel pellets released approximately 20 percent of the krypton during irradiation whereas the fine-particle fuel pellets released less than 1 percent, an apparent anomaly that is being further investigated.

Measurement of dimensions and densities of specimens from the MGCR-2 capsule is complete. The diametral cracks observed in the 1.68-inch-diameter bentonite-containing specimens from the hotter portion of the capsule are believed to have resulted from the difference in thickness expansion as a function of radius. Preliminary evaluation of the room-temperature thermal-conductivity changes for the specimens containing bentonite indicates that the conductivity of pieces from the cooler end of the capsule retained approximately 20 percent of the original value and pieces from the hotter end retained approximately 25 percent.

In the study to determine the effect of a fatigue mechanism on BeO materials, the testing of BeO bars machined from production-type BeO block was completed. Results indicate that a fatigue mechanism will not cause failure of EBOR BeO blocks in the temperature range 1000° to 1600°F if the pieces are repeatedly subjected to a maximum stress of less than 85 percent of the anticipated uncycled modulus of rupture.

Absorber-materials capsule MGCR-7, which has been under irradiation in the Engineering Test Reactor (ETR) since November 9, 1962, had accumulated 2350 hours of irradiation as of May 27, 1963.

CONSTRUCTION ENGINEERING

During the quarter, the AEC office in Washington, D. C., granted a release for construction of the facility and the AEC Idaho Operations Office released the plans and specifications to the construction contractor on June 5, 1963.

All major pieces of equipment to be purchased by General Atomic are on order.

TENTATIVE DESIGN DATA

Site

Location	NRTS, Idaho

Operating Data

Reactor thermal power	10 Mw
Reactor heat flux (max.)	210,000 Btu/hr-ft^2
Reactor heat flux (avg.)	77,100 Btu/hr-ft^2
Reactor outlet coolant pressure	1,089 psia
Reactor inlet coolant pressure	1,107 psia
Reactor inlet coolant temperature	750°F
Reactor outlet coolant temperature	1,275°F
Maximum cladding temperature (hot spot)	1,500°F
Coolant mass flow rate (through core)	14.5 lb/sec
Coolant maximum velocity	240 ft/sec

Reactor Pressure Vessel

Inside diameter	116 in.
Inside height	280 in.
Total weight of pressure vessel and internals	440,000 lb

Reactor Core

Approximate dimensions	23.3 in. × 23.3 in. × 76.0 in. high
Reflector thickness	~7 in. of BeO
Number of fuel elements	36
Number of control rods	4
Loadings:	
U^{235}	100 kg
U^{238}	60 kg
Be/U^{235} atom ratio	117
Composition (with fuel elements in core):	
UO_2-BeO fuel compacts	11.8 vol-%
Cladding and spacers	3.0 vol-%
Shroud	0.6 vol-%
Fuel cooling void	11.0 vol-%
Instrument tube and void	1.6 vol-%
Moderator spine and outer block	63.6 vol-%
Outer spacing gap	8.4 vol-%

Fuel Element (annular ring of rods)

Number of rods	18
Number of fueled rods	18
Rod outside diameter	0.375 in.

Fuel Element--continued

Structural material	Hastelloy-X
Amount of diluent (BeO) in fuel body	76.0 vol-%
Fueled length	76.0 in.
Over-all length of assembly	82.5 in.
Design life at full power	10,000 hr
Burnup at end of life	2×10^4 Mwd/tonne of U

Nuclear Data

Core nuclear constants at operating temperatures:	
Median fission energy	34 ev
Age to indium resonance energy	131 cm^2
Infinite-medium resonance-escape probabilities to 2 ev:	
P_{28}	0.839
P_{total}	0.147
Reactivity (unrodded):	
Hot, clean	1.053
Cold, clean	1.078
Control-rod worth, hot, clean reactor (all four rods)	21.6% $\delta k/k$
Power distributions (normal):	
Axial maximum-to-average factor	2.27
Radial maximum-to-average factor	1.22
Core-element maximum-to-average factor	1.26
Hot-spot factor	3.05

II. REACTOR

CORE AND ASSOCIATED COMPONENTS

Research and Development

Source Element

Work was initiated on the design of the source element to be used in reactor startup. A review of the requirements for the source element revealed that one 50-curie Po-Be source will be required. It was determined that four locations must be available for placement of the source element. These locations will be the four tipping reflectors on the inner row located nearest to the pressure-vessel concentric duct. A meeting was held with a prospective vendor to determine the information required in the specification for the source element. A specification will be prepared based on results of this meeting and on information from other vendors.

Tipping-reflector-model Tests

During the quarter, design and procurement action was initiated for the first phase of the tipping-reflector-element test program. Phase I will consist of room-temperature mechanical tests of the tipping mechanism to provide confirmation of the dynamic performance of the element with emphasis on the resistive frictional forces between unlubricated sliding surfaces. Components of the tipping mechanism and the top-support structure that influence the tipping action will have actual tipping-reflector-element dimensions, finish, and materials. The thermally actuated joint in the design element will be replaced by a mechanically actuated joint for the test element. The weight, center of gravity, and rotational moment of inertia of the column of BeO blocks and disks will also be simulated. In the tests, falling and rotational times will be measured and the dynamic behavior of the specimen during the tipping process will be investigated.

The design of the test model and apparatus is complete and fabrication is in process.

Fuel-pin Tests

A new series of environmental tests of fuel-pin specimens clad with Hastelloy-X-280 was initiated during the quarter. Each of six 15-inch-long

fuel-pin specimens was made with Hastelloy cladding from a separate lot of the production tubing to obtain random sampling of the production order. The simulated fuel pellets were made with production dimensions (with the shallow circumferential groove) and are composed of depleted 57 UO_2–43 BeO (volume-percent uranium). The six specimens have been fabricated and are awaiting creep-shrink treatment.

The mock fuel pellets in four of the six pins are within the dimensions specified for production pellets. The fifth pin was assembled with pellets that were rejected because they failed to meet the requirement of end-squareness. This pin will demonstrate the sensitivity of the thermal-ratcheting mechanism to end-squareness. The sixth pin contains alumina pellets slit normal to the pellet axis at one end of the groove. This pin is intended to demonstrate the effect on cladding performance of pellet fracture of a type (1) that shortens the pellet length and (2) that might result from a stress concentration at the side of the groove.

The six specimens will be creep-shrunk with their longitudinal axes horizontal in two test autoclaves using production-process parameters. None of the fuel pellets was outgassed during fabrication; fuel-pin internal pressure will be monitored during creep-shrinking to measure the amount of gas evolved as a result of contaminants remaining on the pellets from the various postfiring fabrication operations. If gas evolution is negligible, the presently required outgassing step may be eliminated.

After creep-shrinking, the six specimens will be subjected to 100 pressure-temperature cycles simulating reactor operation. Each cycle will be conducted in a helium environment, between 250° and 1600°F temperature, and between ambient and 1200 psia pressure. Fuel-pin internal pressure will be monitored as in previous tests to detect cladding failure. The pins will be inspected dimensionally and X-rayed after each tenth cycle.

Core Thermal Performance

Thermal-performance studies of the 36-element core have been completed. The performance is based on the steady-state design point with start-of-life power generation. An analysis of the maximum fuel-cladding temperature based on hot-spot factors has also been completed.

The total power produced at the steady-state design point with start-of-life power generation is 10 megawatts, of which 9.6 megawatts are produced in the core and 0.4 megawatt in the vessel and internal components. The reactor-coolant flow is 14.53 pounds/second at 750°F and 1120 psia. The core-coolant flow is 13.78 pounds/second with a core-coolant entering temperature of 770°F. The difference between the total reactor-coolant

flow rate of 14.53 pounds/second and the core-coolant flow rate of 13.78 pounds/second is the result of bypass leakage at the top head, core and reflector seals, and support grid. The mixed-mean coolant outlet temperature from the core is 1300°F, and at the reactor outlet duct the temperature is 1270°F; the reactor-coolant outlet temperature is less than the core-coolant outlet temperature, since it was assumed that the bypass-leakage flow did not absorb heat from the core or vessel. The over-all reactor pressure drop is 18.1 psi.

The core elements are orificed to produce approximately the same maximum fuel-cladding temperature of 1530°F. Within a quadrant the coolant outlet temperature differs for each individual core element, with a temperature of about 1230°F for the coolest element and 1400°F for the hottest. This scheme of orificing was necessary to limit the maximum value of the fuel-cladding temperature, since an orificing scheme based on a constant coolant outlet temperature from each element would have resulted in an appreciably higher maximum fuel-cladding temperature in several of the core elements where the pin-to-pin power variation is as much as 25 percent. The reflector elements are orificed for a constant coolant outlet temperature of 1300°F.

The hot-spot analysis for the EBOR core assumed that each uncertainty was based on a 95 percent confidence limit, or, in other words, the odds were 1:20 that the uncertainty would have a larger value than assumed. The uncertainties were applied to one element of the core in such a way as to increase the fuel-cladding temperature while the other elements were unaffected by the particular uncertainty. At the axial location in the element where the temperature is a maximum, the circumferentially averaged fuel-cladding temperature for the average-power fuel pin is 1354°F and the circumferentially averaged temperature for the maximum-power fuel pin is 1530°F. The maximum circumferential fuel-cladding temperature for the maximum-power fuel pin is 1572°F and occurs at the minimum distance between the fuel cladding and the spine. The results of the individual uncertainties are tabulated below:

Uncertainty	ΔT, °F
Radial-flux uncertainty of 10%	82
Fuel-pin-power uncertainty of 25%	45
Heat transfer decreased by 8%	29
Total core-power uncertainty of 3%	25
Element flow area decreased by 3.5%	14
Fuel-pellet-loading variation of 3%	12
Inlet-coolant-temperature uncertainty of 1%	7
Orifice-setting variation of 5%	2

Combining these uncertainties in such a way that their effects are cumulative yields a maximum fuel-cladding temperature of 1808°F. Combining these uncertainties statistically yields a maximum fuel-cladding temperature of 1675°F; the odds in this calculation are 1:20 that the maximum fuel-cladding temperature will exceed 1675°F.

The results of the thermal analysis are being incorporated into the safety analysis report and will eventually be summarized in a topical report.

Construction and Procurement

Core and Reflector Elements

Design proposals were prepared for the coolant-inlet-orifice inserts for the reflector elements. The designs are based on the criterion of removability at site. For a 36-element core, the proposed orifice hole is 0.090 ±0.001 inch for all reflector elements. This will produce outlet-gas temperatures between 1270° and 1350°F. If the number of core elements is increased from 36 to 44, the coolant-inlet-orifice inserts can be replaced. The designs are presently being reviewed.

Information received late in the quarter from several suppliers of parts to be used in assembling the core and reflector elements indicates that the parts will be late in delivery. The information was received too late for proper evaluation of how these late deliveries will affect the assembly of core and reflector elements. Early in the coming quarter, a new schedule will be established which will indicate the pacing items and the effect of the late deliveries on the over-all assembly schedule.

Control Element

Bids were received from seven vendors on the dysprosia tiles for the control element. The purchase order was awarded to Coors Porcelain Company.

Investigations to select a method of welding the control-element panels continued. A design was suggested which could use resistance welding, a method believed to produce minimum distortion. As an outgrowth of the investigation, Airline Welders of Los Angeles, California, was asked to make recommendations for reducing welding distortion in the control element.

Fuel Fabrication

Four pellet-fabrication trial runs have been completed to date, of

which the last three were made during the quarter. During the first three runs, various parameters were changed so that, in effect, four processes were developed to the production stage for each run. The fourth trial run was made using a single standardized process during the entire sequence. A total of 5500 pellets was fabricated in the fourth run from seeded UO_2 and as-received BeO. Yields from the second and third runs were 2600 and 4200 pellets, respectively.

The entire pellet-fabrication process, including the pellets produced from the fourth run, is presently undergoing evaluation. From the various binding materials tested in the four runs, ethyl cellulose has been selected for use in seed preparation and polyvinyl alcohol for use in mix preparation.

PRESSURE VESSEL AND ASSOCIATED COMPONENTS

Research and Development

Pressure-vessel Flow Model

The pressure-vessel flow model has been fabricated and delivered to General Atomic. Delivery of the model was delayed because of difficulties encountered by the vendor in forming the Plexiglas shells to the specified tolerances. Dimensional checks of the completed and assembled model indicate, however, that the flow-passage tolerances are well within the specified values.

In accordance with the purchase requisition for the model, a hydrostatic test was performed by the vendor prior to delivery. The test consisted of pressurizing the model with water to a maximum of 30 psig in increments of 5 psig. Strain-gage instrumentation was installed on the model at three points and monitored during the test. The stresses developed in the model under pressure were determined to be acceptable for the anticipated pressure level during actual testing. A complete visual inspection of the model was made while under hydrostatic pressure. The results of the inspection were satisfactory except for leaks that occurred at two out of eight similar locations, where components were fastened together by bolts. A post-test inspection of these bolt locations indicated that the leaks could be easily corrected by additional sealing of the bolt threads.

The coolant flow in the EBOR pressure vessel is divided into two streams: the main stream, which is about 80 percent of the total flow, and the bypass stream, consisting of the remaining 20 percent. The main stream cools the upper head region, the core-barrel structure, and the core support structure. The bypass steam is orificed to the passage that cools the lower vessel shell and lower head region. Both streams join in

the vessel lower plenum prior to flowing through the core. To measure the amount of bypass flow in the model, a special flow meter was designed for installation at the orifice location in the lower head, which separates the vessel bottom-head coolant passage from the lower plenum region. It was necessary to design the special meter, an area type with an indicating "float," because of space limitations in the model. The meter has been fabricated and is presently being installed in the model.

The model test loop is approximately 50 percent installed, including pump and reservoir-tank installation and piping installation up to the point where it connects to the model.

The pressure-vessel model has been installed in the stand and work is proceeding to install the remaining loop-pipe connections.

The model is being set up for calibrating the bypass flow meter. Since this meter was designed especially for this application, it is to be calibrated in place using the main-loop flow meter as the calibrating standard.

Construction and Procurement

Pressure Vessel and Internals

During the quarter several reports and procedures were received from Pacific Coast Engineering Company (PACECO) and returned with approvals noted. The approved items included:

1. Report R-3, Rev. 3, Shell.
2. Report R-5, Rev. 1, Core Barrel and Thermal Shield.
3. Report R-6, Rev. 1, Thermal Stress and Fluid Flow.
4. Report R-7, Rev. 2, Lower Head.
5. Report R-9, Rev. 3, Vessel Supports.
6. RP-201, Rev. 1, Weld Repair Procedure.
7. RP-202, Temporary Attachments.
8. RT-302, Rev. 2, Radiograph Procedure.
9. SR-602, Rev. 2, Thermal Stress Relief Procedure.
10. Forging Material Specification.
11. Drawing 5060-116E, Rev. 1, Alignment Details.

During the quarter the following major steps in the fabrication of the pressure vessel were accomplished:

1. Pressure-vessel top head: The top-head flange and dish forging were received. The dish forging was dimensionally inspected and found to be acceptable. The top-head flange is ready for dimensional inspection. The top-head flange did not pass the tensile requirements of ASTM-336F2 and was re-heat-treated

by the supplier. The new tensile tests on the forging passed the requirements of the specification.

2. Pressure-vessel shell: The pressure-vessel shell flange was received, dimensionally inspected, and found to be dimensionally acceptable. The pressure-vessel shell halves were returned to the mill for reworking because the out-of-roundness exceeded the purchase-order requirements. Layout of the longitudinal trim lines was made and the halves are ready for burning and bevelling of the seams.

3. Pressure-vessel bottom head: The gore and dollar-plate seams were welded using Manual Welding Procedure WP-35. Radiographs showed that all seams were acceptable. The bottom head skirt is ready for trimming. A low spot on the bottom head was repaired by welding, and radiographs showed the repair to be acceptable. The ASME Code inspector also ruled the repair to be acceptable.

4. Thermal-shield top head: Welding of the gores and dollar plate of the thermal-shield top head was completed using Manual Welding Procedure WP-35. The head is ready for trimming and machining.

5. Thermal-shield course C-1: Course C-1 was rolled to diameter, seam-welded, and released for machining.

6. Thermal-shield course C-2: This course was rolled to diameter and seam-welded using Manual Welding Procedure WP-35. The course is ready for welding to course C-1.

7. Thermal-shield course C-3: The longitudinal seams of this course were welded using Automatic Welding Procedure WP-34. Seam runoff tabs were cut from the trim material and welded as an extension of each longitudinal seam. One of these tabs was sent to General Atomic for evaluation of the impact properties of the weld material.

8. Core-support top head: The gore and dollar-plate seams were welded using Manual Welding Procedure WP-35. Radiographs revealed a defect in one of the seams. Repair was made in accordance with the approved procedure. The repaired area has been approved.

9. Core-support-shell course C-1: The three pieces comprising this course were welded together and rolled to diameter, and the final seam was welded. The three longitudinal seams of this course were radiographed and no defects were found.

10. Core-support-shell course C-2: This course was rolled to diameter and measurements were taken on roundness, diameter,

and offset of the seam. All measurements were found within tolerance. The single longitudinal seam was welded using Manual Welding Procedure WP-35. Radiographs revealed no defects.

11. Core-support-shell course C-3: This course was rolled to diameter and the single longitudinal seam was welded using Manual Welding Procedure WP-35. Radiographs revealed no defects.

12. Core-support bottom head: The gores and dollar plate of the bottom head were welded using Manual Welding Procedure WP-35. The head has been laid out for trimming.

The first installment of "Data Book for the Design and Fabrication of the EBOR Pressure Vessel and Associated Components" (GA-4136) was issued. The purpose of the data book is to document the design and fabrication of the pressure vessel and associated components. The data book includes sections entitled Engineering Design, Material Procurement, Manufacturing Planning and Qualification, Manufacturing Operations and Inspection, Equipment Testing (Vendor), Shipment, Site Receiving Inspection, Equipment Installation and Inspection, Equipment Testing (Site), and Materials Surveillance Program.

The Engineering Design section will contain the following information:

1. A physical description of the pressure vessel and internal components, utilizing an isometric drawing of the components.

2. A statement of the design requirements referencing the purchase-equipment specification.

3. A description of the material requirements, which define the allowable stresses and identify the mechanical and thermal properties of the construction materials.

4. A discussion of the Phase I steady-state analysis, including a description of the approach to the analysis, the logic of the analysis, and the methods of analysis and stress, temperature, and pressure-drop summaries of the results of the analysis.

5. A description of the Phase II fatigue analysis, including a discussion of the approach to the analysis, method of analysis, cases analyzed, and results of the analysis.

6. A description of the significance of the hydrostatic and reactor site tests performed on the equipment.

7. An appendix which includes the construction drawings and reference to the analysis reports.

Concentric Duct and Anchor

Comments were returned to the supplier, Dravo Corporation, on the preliminary analysis of the concentric duct and internal insulation. The internal insulation will be supplied by Solar Aircraft Company of San Diego, California. A final report was received from Dravo Corporation on the design and construction of the concentric duct and anchor. The report is presently being reviewed.

CONTROL-ROD-DRIVE MECHANISMS

Construction and Procurement

Latch Assembly

The latch assembly was modified to permit a limited amount of rotation between the drive and the control element. This was accomplished by eliminating the rigid joint and modifying the thread arrangement so that the control-element lift now has an external thread. To reduce the possibility of self-welding, the external threads of the control element will be flame-plated with tungsten carbide. The mating part of the internal thread will be made from Haynes-25 material.

Scram Motor

The pacing item among the vendor components for the control-rod-drive mechanism is still the scram motor, being supplied by Lear Siegler, Inc. This component is now scheduled for delivery by the end of July, 1963.

Prototype Tests

The prototype tests of the control-rod-drive mechanism are planned to begin early in August. The purpose of the tests is to confirm that the changes made from the experimental drive to the production drive will not affect the reliability and performance of the drives.

COMPONENT HANDLING

Construction and Procurement

Control-rod-drive Transfer Cask

Construction of the control-rod-drive transfer cask was completed by the supplier, U.S. Nuclear Corporation, and the component has been received at the Idaho site.

STF-bridge Modification

An inspection of the existing assembly at the Idaho site was made by the vendor, Todd Shipyards. The operation of the bridge was found to be erratic but was corrected by General Atomic personnel. The vendor started arrangements for disassembly of the instrument bridge early in June. Several General Mills drawings on this equipment were requested by the vendor. Most of the drawings have been obtained from individuals formerly associated with operations of the Shield Test Pool Facility.

INSTRUMENTATION

Research and Development

The design is complete for dummy in-core instrumentation connectors. These connectors will be used during the construction phase to check out in-core wiring.

The pneumatic activation loop in the General Atomic TRIGA facility is being investigated for testing the EBOR failed-fuel detection precipitator under functional conditions. Qualitative results can be obtained with the precipitator under these conditions. The feasibility of quantitative calibration is the area of concern in the investigation.

Construction and Procurement

The status of EBOR instrumentation construction and procurement activity at the end of the quarter is given below:

1. Fabrication of the nuclear and safety system is complete. Testing and inspection are 98 percent complete.
2. Fabrication of the control panelboards is 70 percent complete; 90 percent of the components have been received.
3. Fabrication of the in-core instrumentation is 40 percent complete.
4. Fabrication of the Inconel-sheathed reactor thermocouples is 75 percent complete.
5. Reworking of AEC-furnished equipment received from the STF facility is complete.
6. A method of utilizing the operational-control-rod instrumentation system during receiving-inspection checkout of the control-rod drives has been formulated. Vendor quotations for adaptive subassemblies have been solicited.

7. All components of the coolant-activity monitoring system have been received and the integrated system has been satisfactorily bench-tested.

8. Fabrication and inspection-testing of the high-pressure-helium instrument valves is complete.

9. The instrument-depressurizing junction boxes, helium-instrument control boards, selector valve manifolds, pressure-vessel thermocouple-cable harness, and failed-fuel detection system programmer are on order.

10. One of the three recorders required for the temperature-monitoring system has been ordered. The two remaining recorders will be obtained by modifying two surplus research and development recorders.

11. Approximately 75 percent of the AEC-furnished materials and subassemblies have been ordered to enable the contractor to install in-core instrumentation.

12. An economical source of metallic radiation shielding in the form of random-size (1/8 to 1/2 inch in diameter), mixed material (chromium steel, carbon steels, and stainless steel reject ball bearings) has been located. This shielding will be used to fill the vertical voids in the three instrumentation conduits that penetrate the biological shield above the reactor vault.

SAFETY ANALYSIS

First drafts of the following subsections of the final safety-analysis report (SAR) were prepared:

Control-rod-drive mechanism - Description, principles of operation, and reliability analysis.

Control-rod-drive mechanism - Basis for selection of top-mounted drives.

The first draft of Section IV, Reactor Core, is approximately 75 percent complete.

The digital computer code for system transient analysis was written during the quarter. Operational analysis will proceed in the following sequence:

1. Perturbations to the design-point full-power condition, including changes to the core-outlet demand temperature, helium-to-air heat-exchanger-outlet demand temperature, valve setting, and scram with main circulator on.

2. Helium inventory reduction on automatic temperature control.
3. System warmup and controlled power changes.
4. Emergency air cooling.

III. REACTOR PHYSICS

NUCLEAR DESIGN

Reactivity Calculations

The reactivity calculations for EBOR were essentially completed during the quarter. Several revisions in the EBOR design were noted in the previous quarterly progress report (GA-4124). The calculations reported here are a continuation of the analysis of the perturbations leading to these revisions. The variation of reactivity with lifetime and the differential control-rod worths at the beginning and end of life were recalculated. To facilitate the presentation of the data, two special computer programs that prepare plots of the data were written using the SC-4020 plotter at General Dynamics/Electronics. The first program produces contour maps of the flux and power distributions from the XY-flux distribution calculated by the 2DXY code. The second program produces axial power, burnup, flux, and nvt distributions for each core and reflector element. These values were calculated from 2DXY radial and FEVER axial fluxes, combined by a simple synthesis of the rodded and unrodded sections of the core. A least-squares fitting technique was used to smooth out the discontinuities between rodded and unrodded sections of the core. No change in the radial-flux distribution with time was assumed in this model. With the strong reflector-moderating effect present, and the small amount of fuel depletion, the radial distributions are not expected to change appreciably during the core lifetime.

The recalculation of the variation of reactivity with lifetime for the 36-element core was performed with the FEVER code, but with compositions and cross sections that were consistent with those used in the final reactivity calculations reported in GA-4124. Table 1 shows a summary of the burnup data for 10,000 hours of full-power operation. Figures 1 to 6 give the axial-power distribution as a function of lifetime in the fuel elements, as obtained by a synthesis with 2DXY results by the technique previously mentioned. Figure 7 shows the numbering scheme used for the elements. The five curves shown on Figures 1 through 6 correspond to five different times during the core operation: 0 hours with equilibrium xenon, 2500 hours, 5000 hours, 7500 hours, and 10,000 hours. A better picture of the power distributions in the EBOR core requires a three-dimensional analysis, which is beyond the capabilities of suitable analytical techniques.

Table 1

SUMMARY OF EBOR BURNUP DATA FOR 36-ELEMENT CORE AFTER 10,000 HOURS OF FULL-POWER OPERATION

Excess-reactivity Requirements, %:	
Fission products	2.47
Heavy isotopes	0.60
Li^6	0.27
Burnup	0.70
Control contingencies	1.23
Total excess	5.27

Isotope Inventories:

	Beginning of Life	End of Life
U^{234}	668 g	636 g
U^{235}	99.6 kg	92.0 kg
U^{236}	462 g	2738 g
U^{238}	59.0 kg	58.3 kg
Np^{239}	0 g	4.3 g
Pu^{239}	0 g	572 g
Pu^{240}	0 g	19.5 g
Pu^{241}	0 g	9.6 g
Pu^{242}	0 g	0.2 g

Burnup at 10,000 Hours:	
Core average, % of pellet destroyed	0.17
Maximum, % of pellet destroyed	0.43
Fast nvt (>1.0 Mev)	
Avg	3.75×10^{20}
Max	1.92×10^{21}
Epithermal nvt (1.0 Mev → 1 ev)	
Avg	1.6×10^{21}
Max	7.7×10^{21}
Thermal nvt (1 ev → 0)	
Avg	2.07×10^{20}
Max	3.76×10^{20}
Fissions/cm^3	
Avg	6.09×10^{19}
Max	1.54×10^{20}

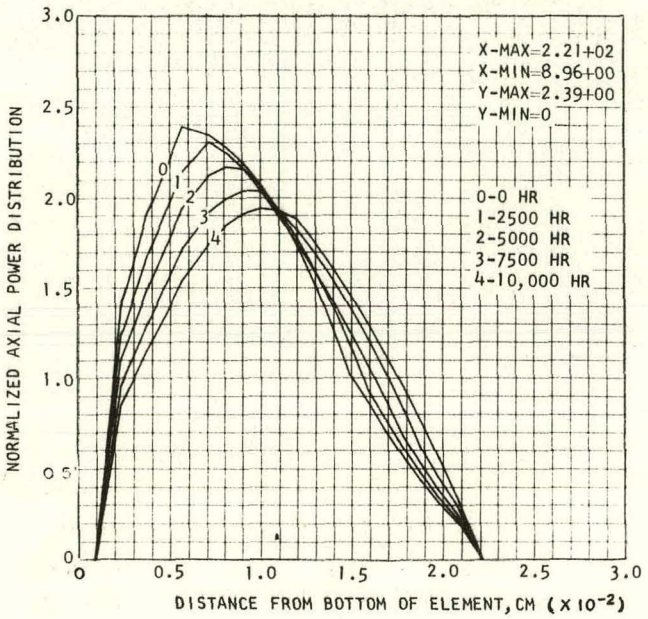

Fig. 1--Power distribution in region 1 for time steps 0 through 4

Fig. 2--Power distribution in region 2 for time steps 0 through 4

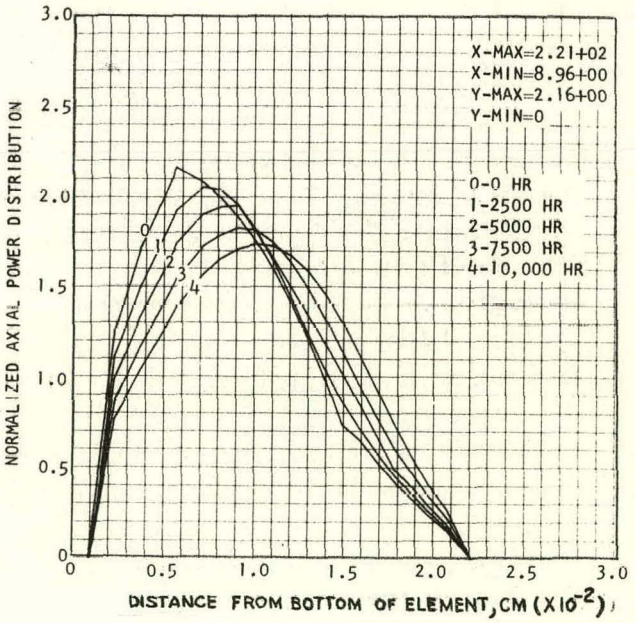

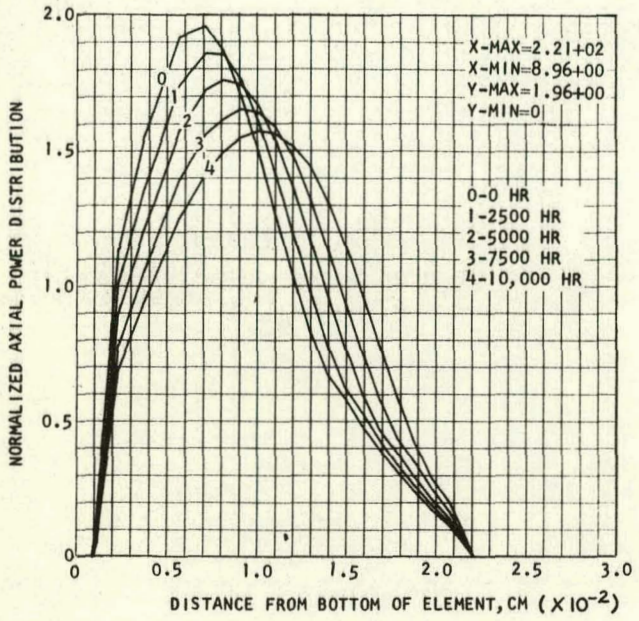

Fig. 3--Power distribution in region 3 for time steps 0 through 4

Fig. 4--Power distribution in region 4 for time steps 0 through 4

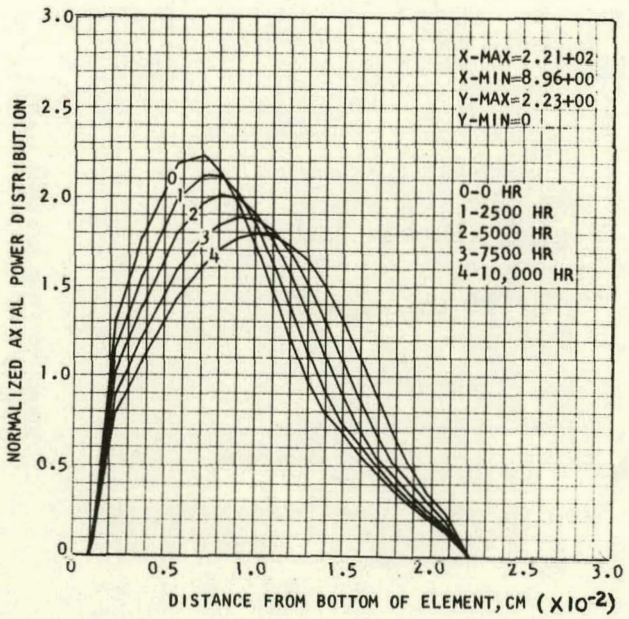

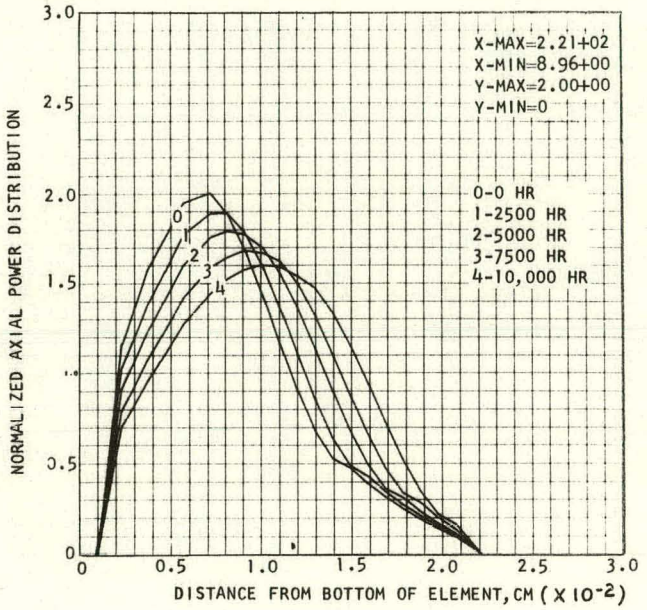

Fig. 5--Power distribution in region 5 for time steps 0 through 4

Fig. 6--Power distribution in region 6 for time steps 0 through 4

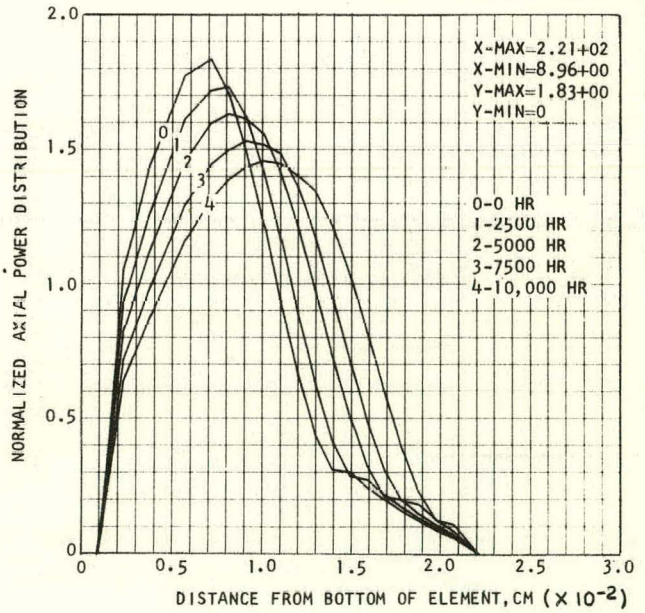

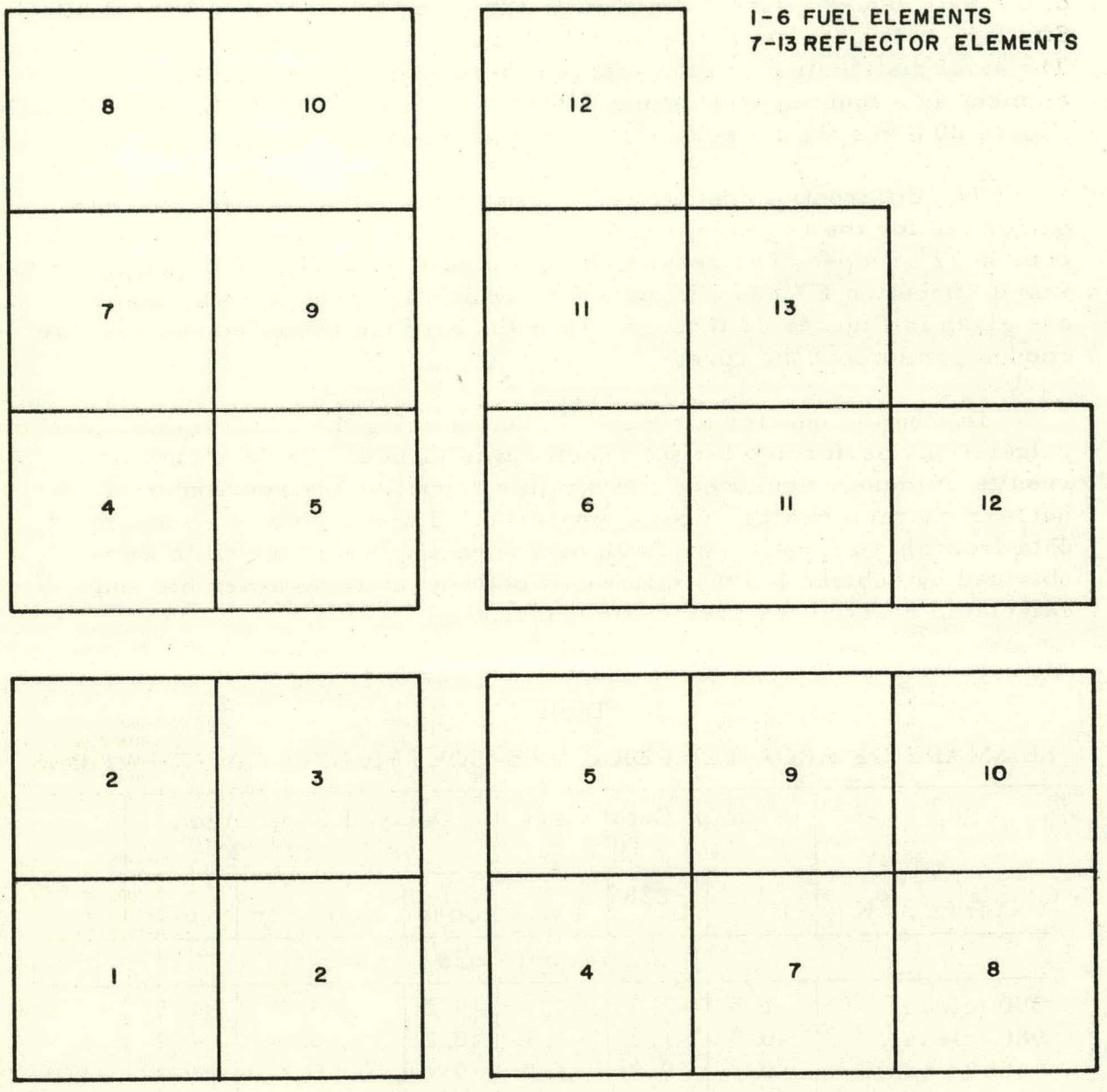

Fig. 7--Numbering scheme for EBOR elements (one-fourth core geometry)

The axial variation of the fast, intermediate, and thermal fluxes and corresponding nvt values as a function of lifetime for element No. 1 (one of the four center elements in EBOR) are given in Figures 8 through 13. Similar curves are available for all of the core and reflector elements. The axial distribution of atom-percent burnup in the fuel for each fuel element as a function of lifetime is given in Figures 14 through 19. Finally, Figure 20 gives the core-reactivity requirements as a function of lifetime.

The differential control-rod worth as a function of insertion was calculated for the beginning- and end-of-life conditions, using the GAZE code in 12 groups. The results are given in Figure 21. Detailed power and flux distribution XY contour plots for the beginning-of-life hot condition are given in Figures 22 through 29 for the average unrodded and average rodded portions of the core.

During the quarter a report[1] summarizing the temperature-coefficient calculations performed for the reactor was issued. Table 2 shows the results of these calculations. A similar report on the remainder of the nuclear characteristics is being prepared. Table 3 gives a summary of data from this report. The "with bias" reactivities in the table were obtained by subtracting the difference between critical-assembly and calculated reactivities previously established.

Table 2

SUMMARY OF EBOR TEMPERATURE-COEFFICIENT CALCULATIONS

	Prompt Coefficient, $\delta k/k \times 10^5/^\circ K$			Delayed Coefficient, $\delta k/k \times 10^5/^\circ K$			
Temp., $^\circ K$	U^{235}	U^{238}	Total	Core	Reflector	Total	Total
36-element Core							
300 (clean)	-1.5	-2.8	-4.3	-0.2	+0.7	+0.5	-3.8
980 (clean)	-0.5	-1.2	-1.7	-0.2	+0.4	+0.2	-1.5
1366 (clean)	-0.3	-0.9	-1.2	+0.0	+0.2	+0.2	-1.0
300 (equil. Xe)	-0.5	-1.1	-1.6	-0.2	+0.3	+0.1	-1.5
980 (end of life)	-0.4	-1.0	-1.4	-0.2	+0.4	+0.2	-1.2
44-element Core							
300 (clean)	-1.6	-2.9	-4.5	-0.2	+0.5	+0.3	-4.2
980 (clean)	-0.5	-1.3	-1.8	-0.2	+0.3	+0.1	-1.7

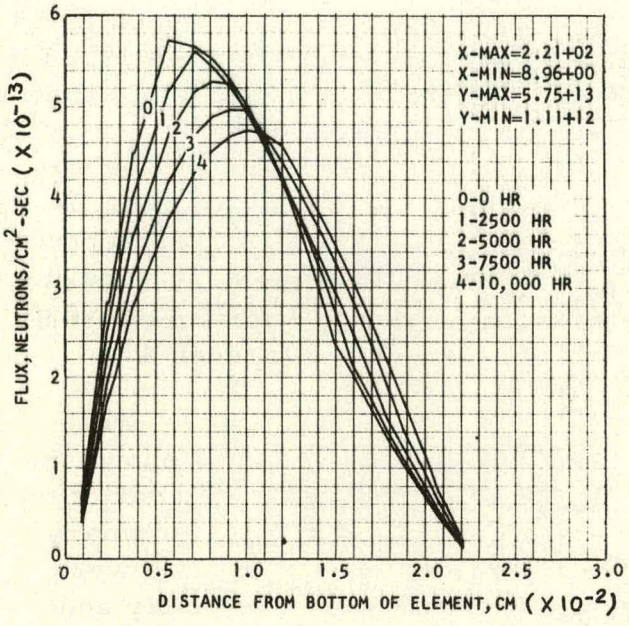

Fig. 8--Flux >1 Mev in region 1 for time steps 0 through 4

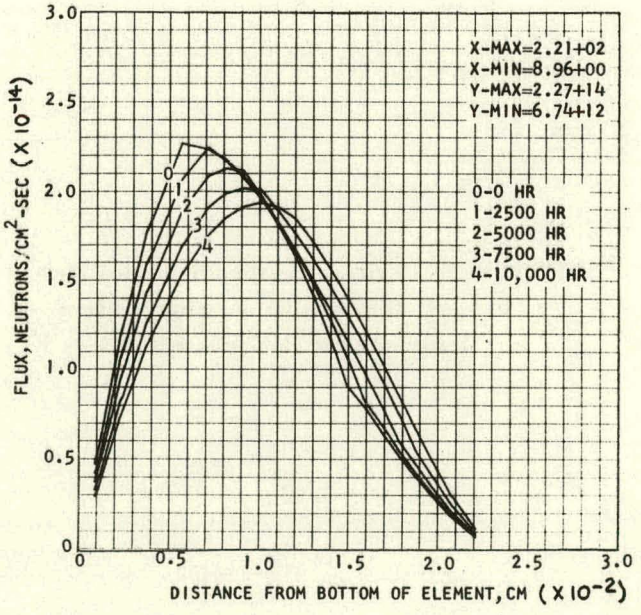

Fig. 9--Flux from 1 ev to 1.0 Mev in region 1 for time steps 0 through 4

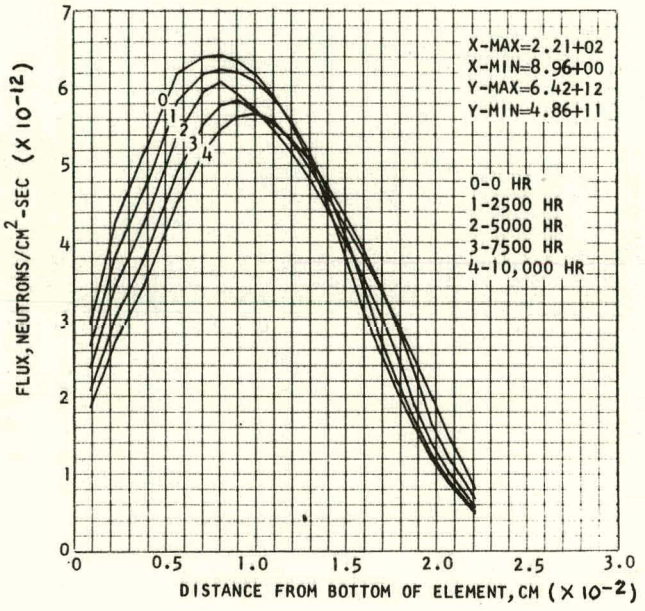

Fig. 10--Flux from 1 ev to 0 in region 1 for time steps 0 through 4

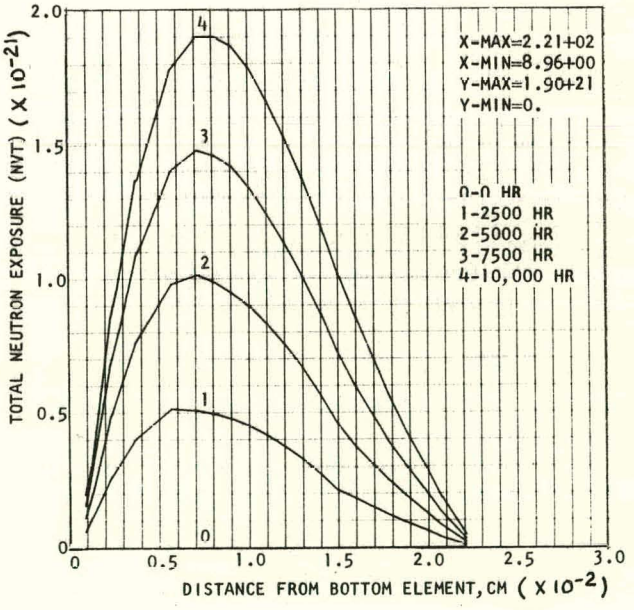

Fig. 11--Total neutron exposure (nvt) >1.0 Mev in region 1 for time steps 0 through 4

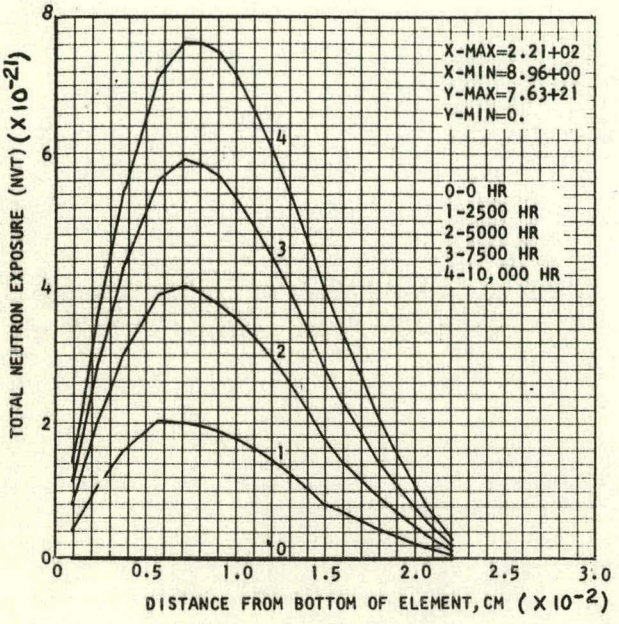

Fig. 12--Total neutron exposure (nvt) from 1 ev to 1.0 Mev in region 1 for time steps 0 through 4

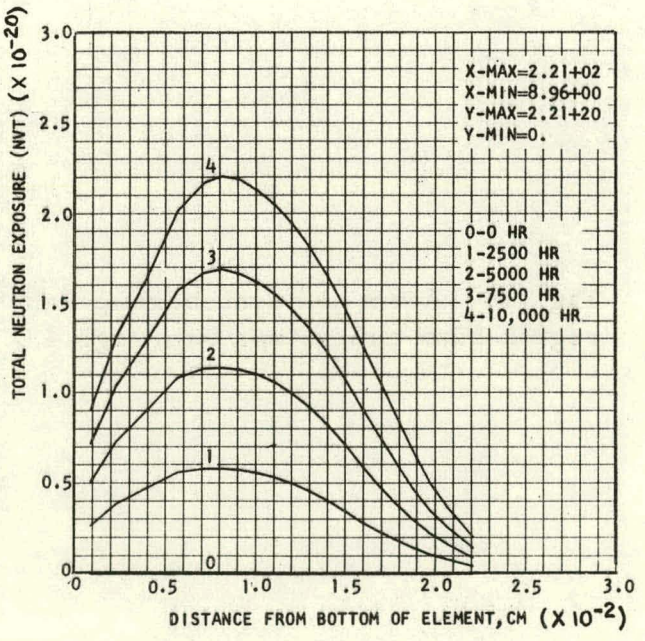

Fig. 13--Total neutron exposure (nvt) from 1 ev to 0 in region 1 for time steps 0 through 4

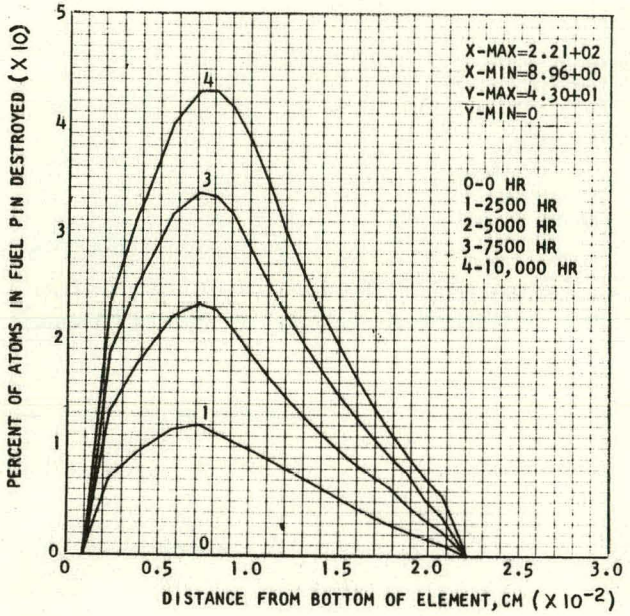

Fig. 14--Atom-percent burnup in region 1 for time steps 0 through 4

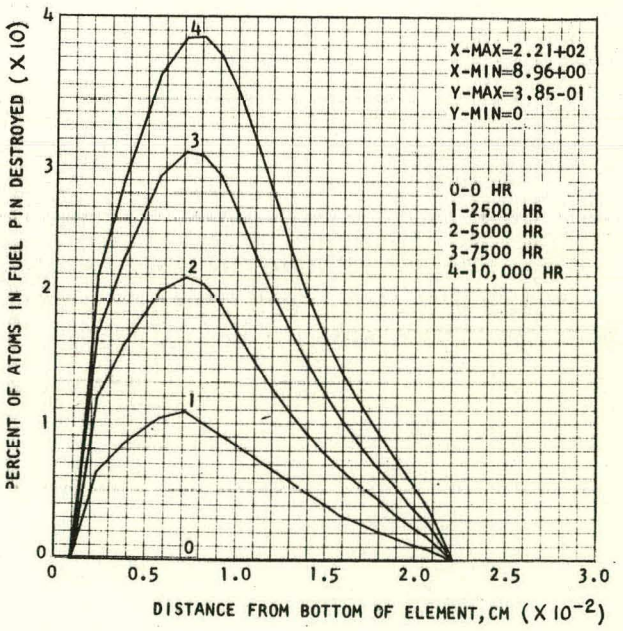

Fig. 15--Atom-percent burnup in region 2 for time steps 0 through 4

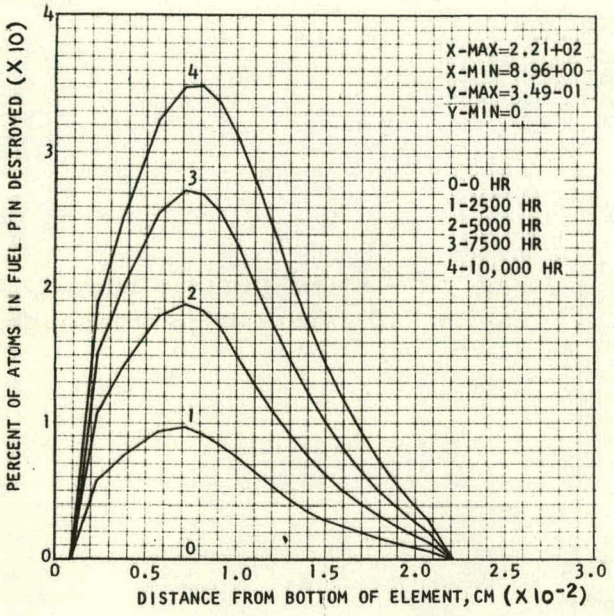

Fig. 16--Atom-percent burnup in region 3 for time steps 0 through 4

Fig. 17--Atom-percent burnup in region 4 for time steps 0 through 4

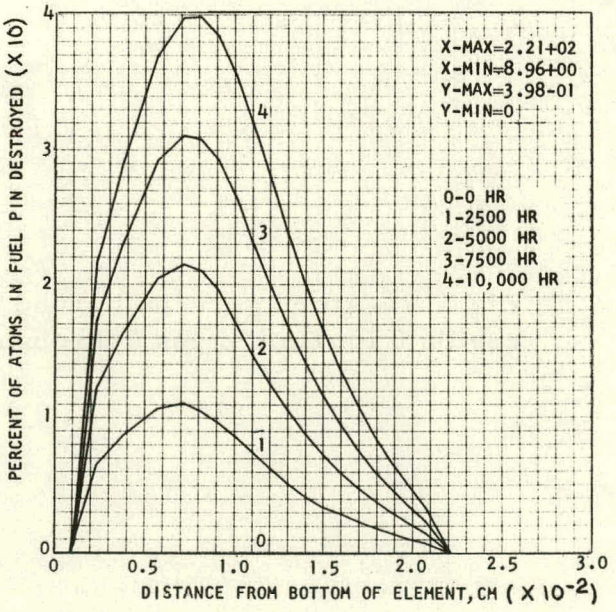

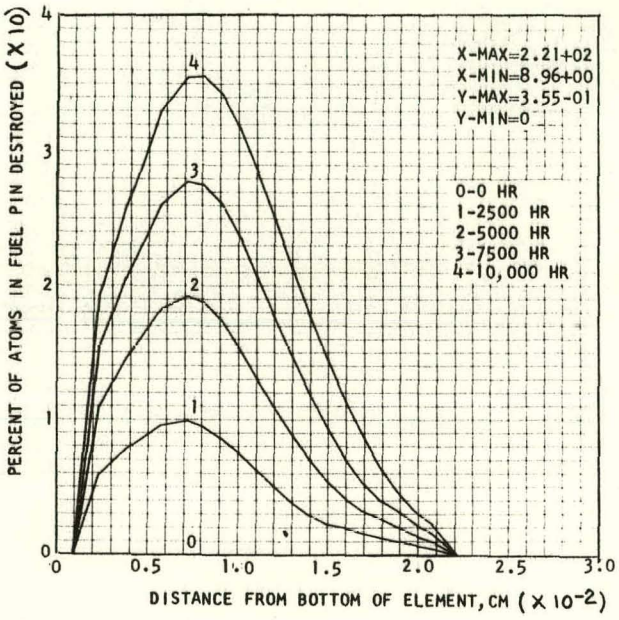

Fig. 18--Atom-percent burnup in region 5 for time steps 0 through 4

Fig. 19--Atom-percent burnup in region 6 for time steps 0 through 4

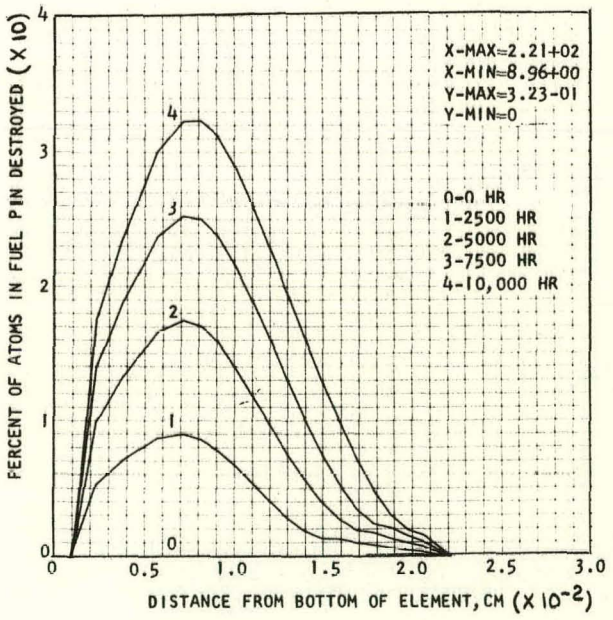

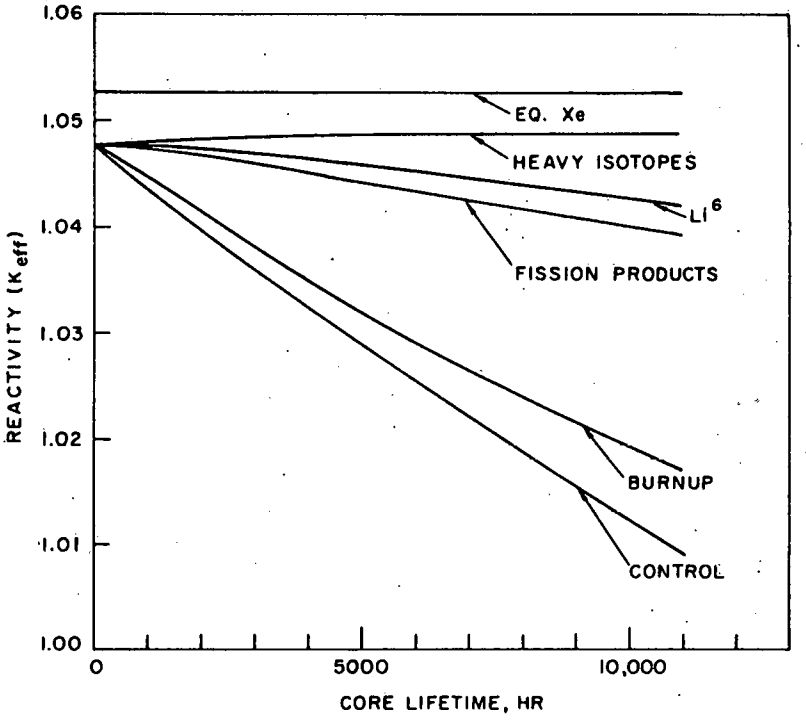

Fig. 20--EBOR reactivity requirements versus core lifetime

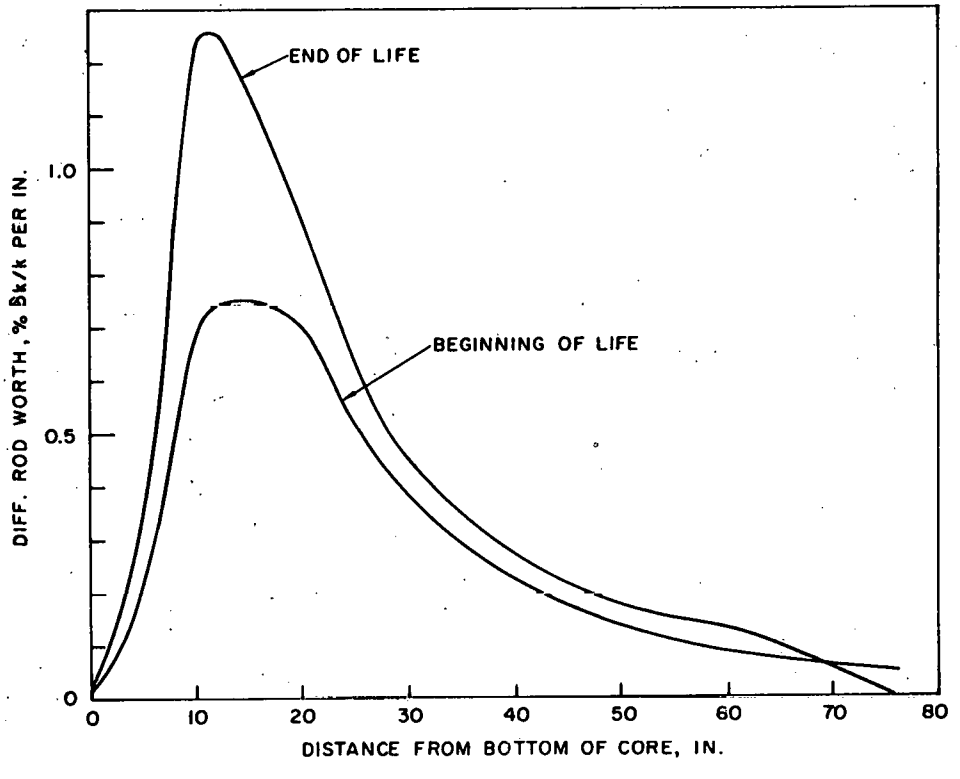

Fig. 21--EBOR rod worth versus insertion for beginning and end of life

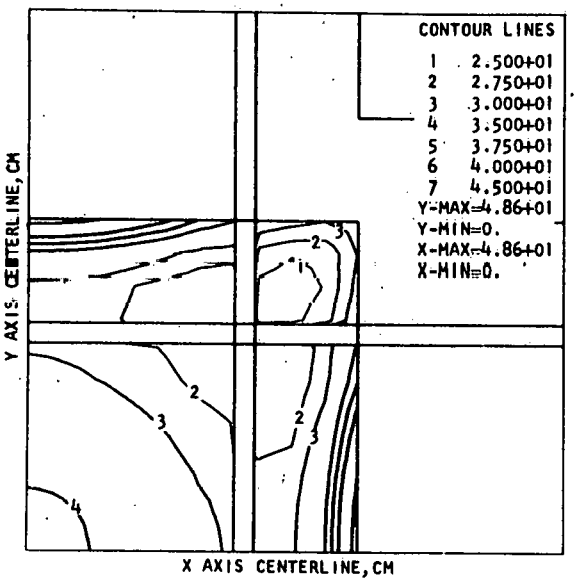

Fig. 22--Contour map of reactor power (in watts/cm^3); unrodded core

Fig. 23--Contour map of reactor power (in watts/cm^3); rodded core

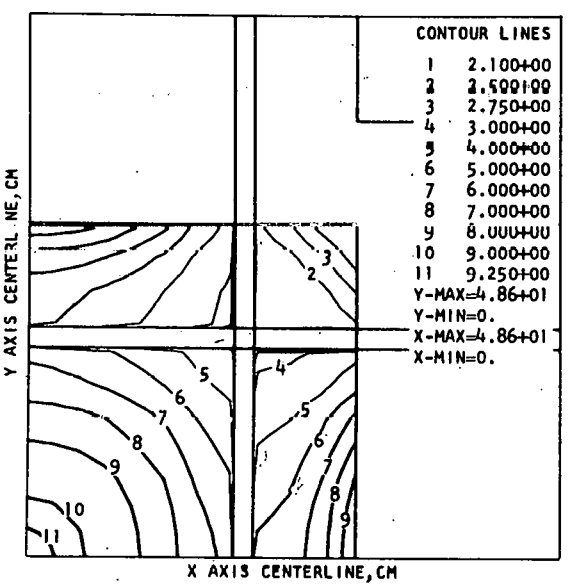

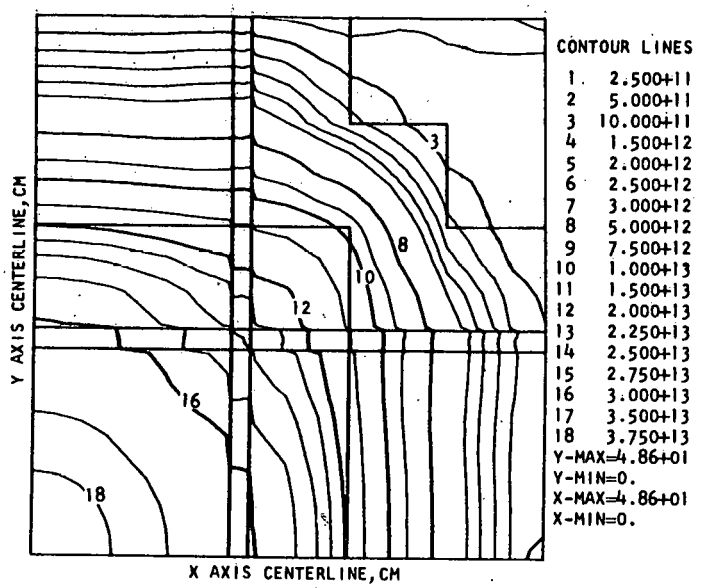

Fig. 24--Contour map of reactor flux (in neutrons/cm^2-sec)>1.0 Mev; unrodded core

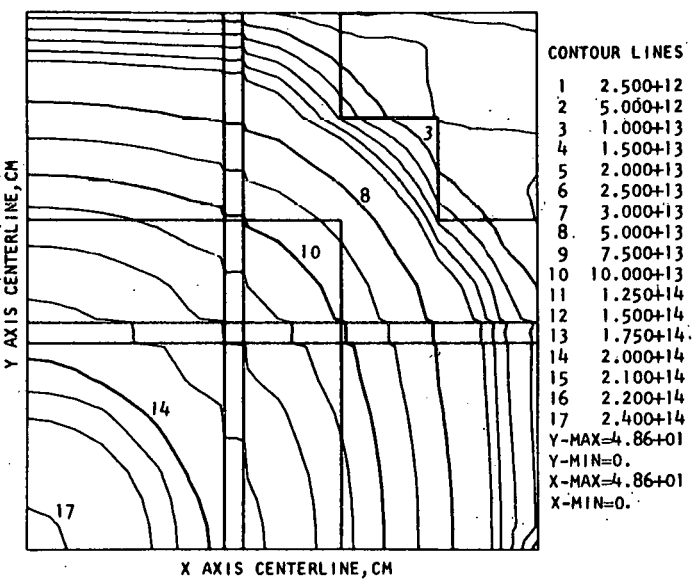

Fig. 25--Contour map of reactor flux (in neutrons/cm^2-sec) from 1 ev to 1 Mev; unrodded core

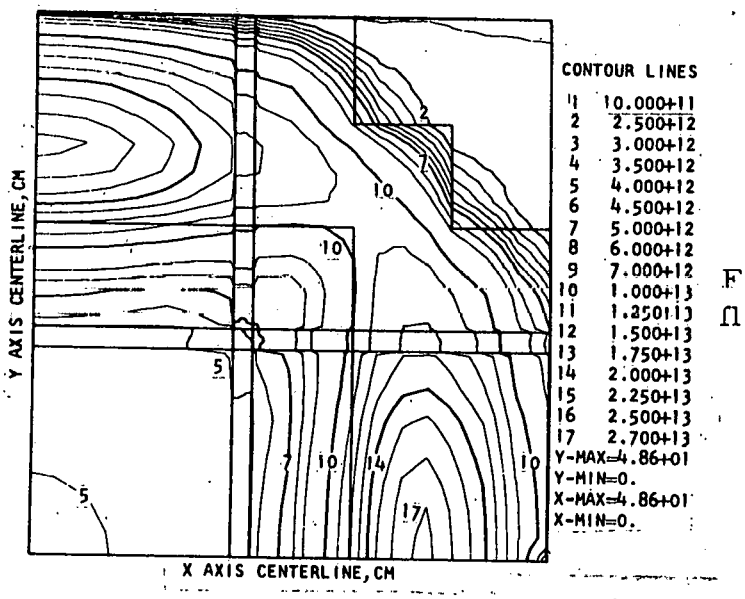

Fig. 26--Contour map of reactor flux (in neutrons/cm^2-sec) from 1 ev to 0; unrodded core

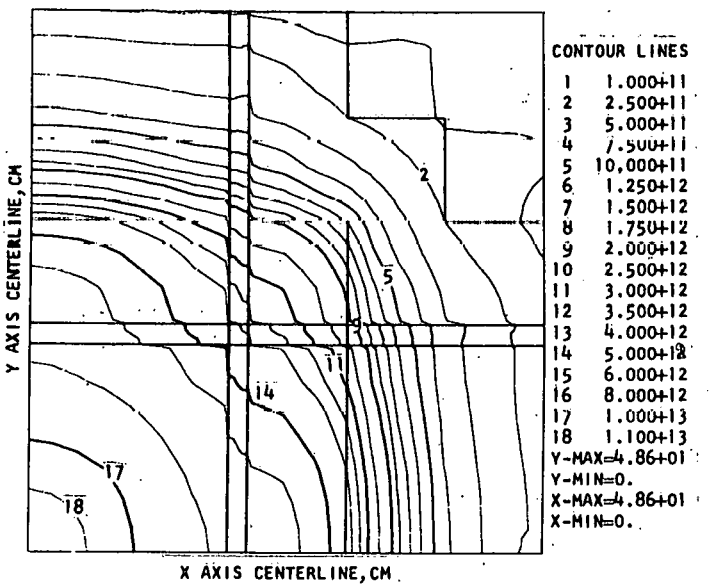

Fig. 27--Contour map of reactor flux (in neutrons/cm^2-sec)>1.0 Mev; rodded core

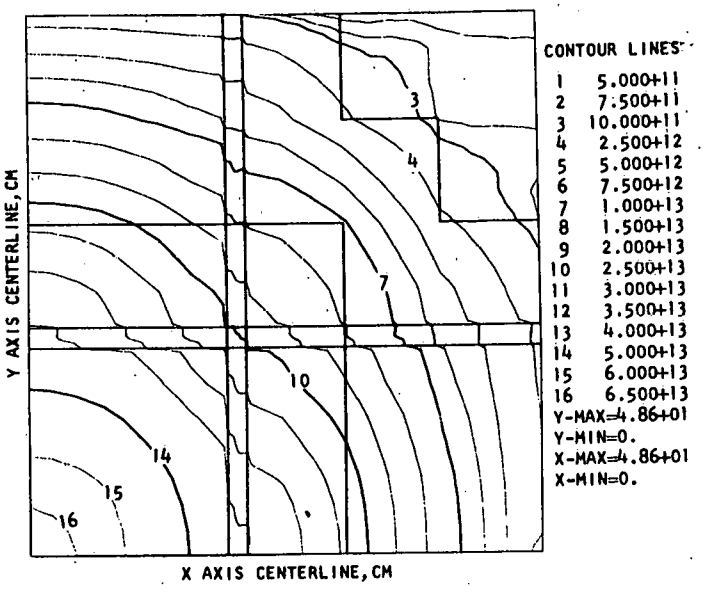

Fig. 28--Contour map of reactor flux (in neutrons/cm^2-sec) from 1 ev to 1 Mev; rodded core

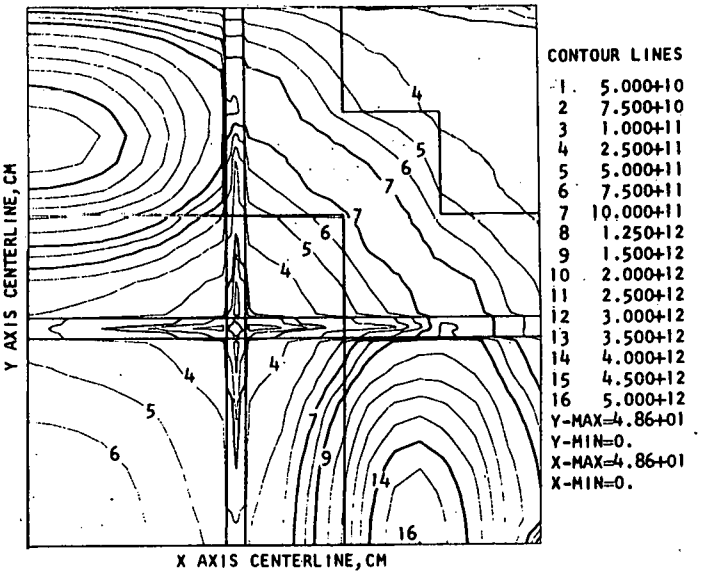

Fig. 29--Contour map of reactor flux (in neutrons/cm^2-sec) from 1 ev to 0; rodded core

Table 3

SUMMARY OF EBOR REACTIVITY CALCULATIONS

Excess reactivity, %:	
Without bias	
Cold	1.0784
Hot	1.0527
With bias	
Cold	1.0622
Hot	1.0369
Hot-to-cold reactivity change	2.26% δk/k

Beginning-of-life control-rod-worth reactivity decrease, % δk/k:

Case	Cold	Hot
All rods out	0.0	0.0
One rod in	4.0	4.0
Two rods in		
Adjacent	8.1	8.0
Diagonal	9.7	9.5
Three rods in	14.2	14.0
Four rods in	21.6	21.3

Kinetics Calculations

Preliminary kinetics investigations were initiated during the quarter to ascertain the nuclear-thermal response to the core following step or ramp insertions of positive reactivity and partial or total loss-of-coolant flow. Neither the possibility nor the credibility of any of the assumed reactivity insertions was considered in this study.

In most of the reactivity insertions studied, it was assumed that no scram action occurred. This is, of course, not realistic but was done primarily to investigate the effect of the calculated prompt negative temperature coefficient and to determine the time required to reach temperatures that would cause damage to the fuel-element cladding, i.e., greater than approximately 2300°F. Future studies will include consideration of the appropriate scram action in the event of such reactivity insertions and will therefore be less severe and more realistic.

For these studies, a model of the fuel element that could be used in a modified version of the BLOOST-2 code was assumed. BLOOST-2 was designed for transient analysis of HTGR-type fuel elements. An EBOR fuel

element is made up of a central moderator spine 2.012 inches in diameter surrounded by 18 fuel pins 0.375 inch in diameter. The spine and fuel pins are surrounded by an outer square, annular moderator block having outer dimensions of 3.514 inches and an inner diameter of 2.906 inches. In the EBOR element, heat is removed by the coolant passing over the fuel pins, i.e., between the spine and the outer moderator block. In the BOOST-2 kinetics-heat-transfer code, heat removal takes place at the outer circumference of the moderator sleeve. It was necessary to modify the code to eliminate the sleeve region entirely in order to simulate heat transfer to the gas at the surface of the fuel region. The model chosen for use with the modified code consisted of a central moderator spine surrounded by an annular fuel region. The dimensions of the model were chosen so that the total moderator and fuel volumes were the same in the model as in the actual element. The model used is shown in Figure 30. The steady-state heat-transfer coefficient and fuel conductivity were increased in the heat-transfer calculations to account for the difference in geometry so that the fuel average and fuel surface temperatures and the coolant-gas temperature would be the same in the model as for the actual EBOR element. The gap thickness of 0.045 inch between the fuel and moderator in the model is the same as that in the actual element.

It was realized that the model would overpredict the moderator temperature. This is of no consequence, since almost all of the negative temperature coefficient in EBOR is prompt and associated with the temperature of the fuel region only.

The following assumptions were made in the analysis:

1. Input data were for an "average" element, i.e., one having an average heat-generation rate and axial distribution and an average coolant-flow rate. No such average element actually exists in the reactor owing to the power-density variation over the core and the fact that the helium is orificed differently to the various elements to maintain a constant cladding temperature for all elements. The axial-power distribution for this element corresponding to 65 percent rod-bank insertion is shown in Figure 31.
2. The delayed-neutron fractions used were the actual fractions for U^{235} as reported by Keepin,[2] and no allowance was made for the "effectiveness" correction to these numbers or for additional delayed neutrons due to the (γ, n) reaction in beryllium.
3. Ramp insertions assumed a rod withdrawal at the rate of 2 inches per minute.
4. All scram action assumed in the analysis was after a 40-millisecond delay time.

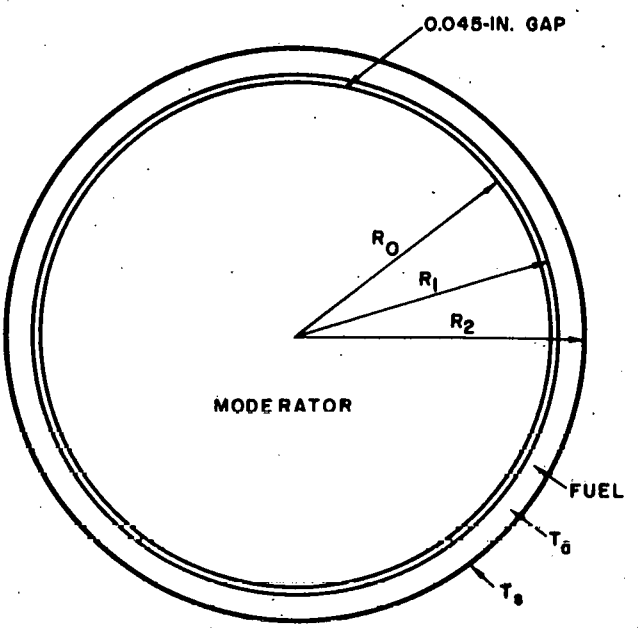

R_0 = 1.618 IN.
R_1 = 1.663 IN.
R_2 = 1.844 IN.

Fig. 30--Fuel-element model used in hazards analysis; fuel average temperature (T_a) and fuel surface temperature (T_S) equal those in EBOR element

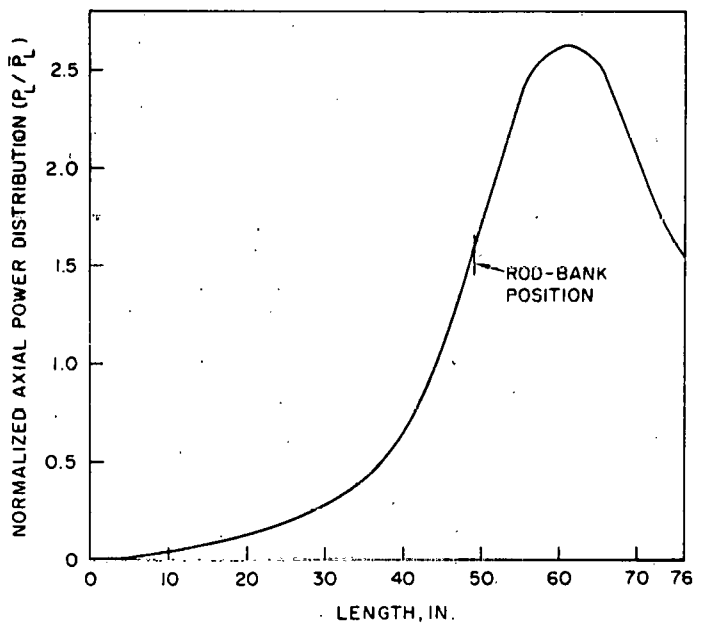

Fig. 31--Axial power shape for model element corresponding to 65 percent rod-bank insertion

Table 4 summarizes the kinetics and heat-transfer input data used in the analysis.

Table 4

KINETICS AND HEAT-TRANSFER INPUT DATA

Kinetics data:		
Neutron generating time	2.2×10^{-5} sec	
Delayed neutron fractions and decay constants	β_i	λ_i
1	0.000211	0.01243
2	0.001402	0.0305
3	0.001254	0.11143
4	0.002528	0.30134
5	0.000736	1.1362
6	0.000269	3.0134
Heat-transfer data:		
Helium coolant-inlet temperature	$770^{\circ}F$	
Steady-state heat-transfer coefficient	1105.0 Btu/ft^2-$^{\circ}$F-hr	
Steady-state flow rate per element	1328.0 lb/hr	
Specific heat of coolant	1.241 Btu/lb-$^{\circ}$F	
Conductivity of fuel body	72.0 Btu/ft-$^{\circ}$F-hr	
Reactor power	10.0 Mw	

The relative, integrated control-rod worth, from which the ramp reactivity insertion rates were determined, is shown in Figure 32. In the ramp analysis it was assumed that the total worth of any one rod from 76-inch to 0-inch insertion was worth 0.06 $\delta k/k$. The calculated EBOR temperature coefficient as a function of temperature is shown in Figure 33. The various components of the over-all coefficient are indicated in the figure and include the prompt coefficient, core delayed coefficient, and the positive contribution due to the reflector delayed coefficient. It is seen from Figure 33 that the most important contribution to the total coefficient is the prompt component. The total coefficient was assumed in this analysis to apply to fuel-region temperatures. That is, it was assumed in the analysis that the calculated total coefficient was the prompt coefficient. This has the effect of underestimating the negative-reactivity cutback due to fuel-temperature increases in a transient and is therefore a conservative assumption.

Three basic types of reactivity insertions were investigated: (1) positive, step reactivity insertion, (2) positive, ramp reactivity insertion, and (3) loss of coolant with no reactivity insertion. In the analysis of the step

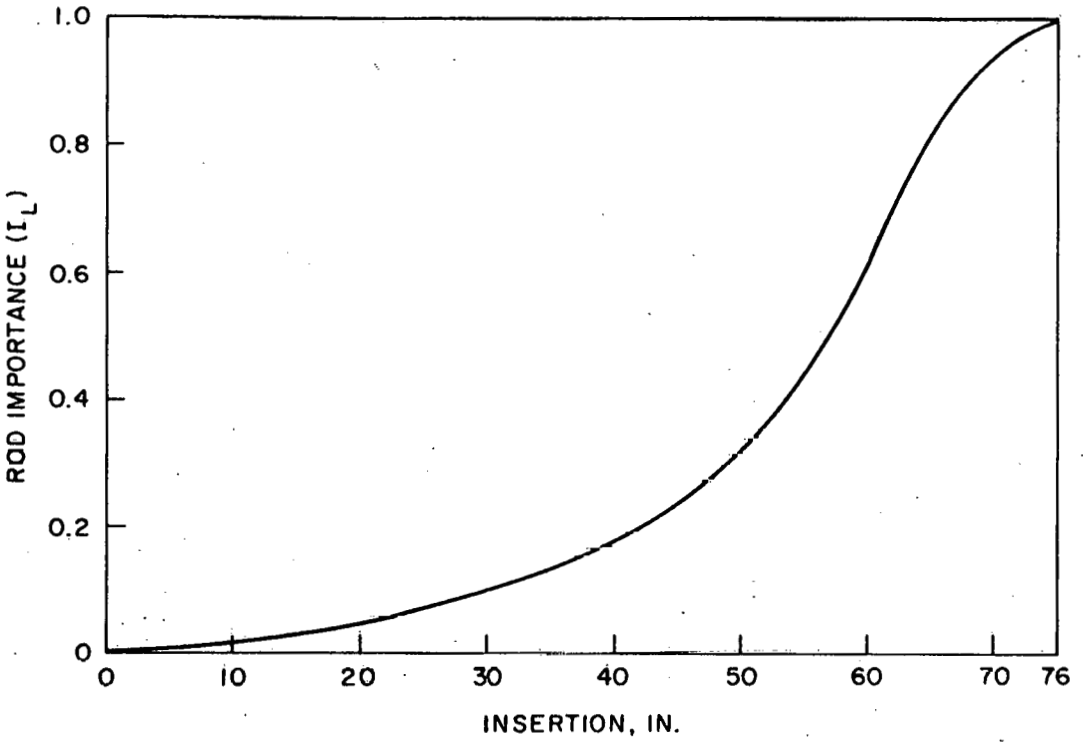

Fig. 32--Integrated axial rod importance versus insertion depth

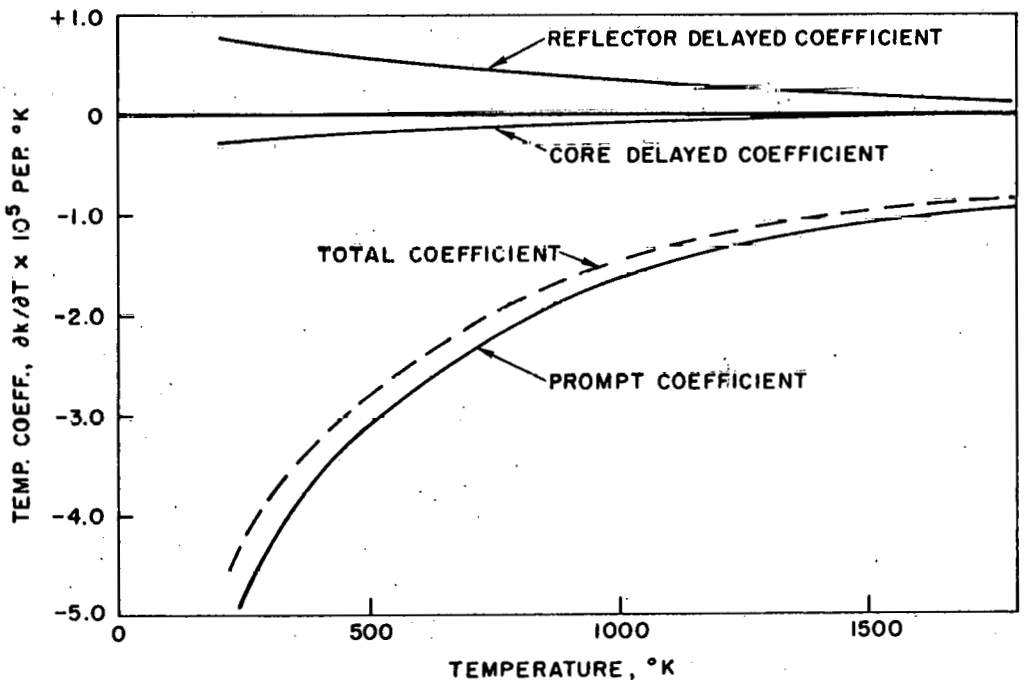

Fig. 33--EBOR temperature coefficient

insertion, studies were performed to determine the maximum step change possible assuming conditions without scram and with scram. Four temperatures were considered important: average helium outlet, average fuel element, hot-spot temperature in the average element, and hot-spot cladding temperature in the average element. It is important to note that these temperatures always refer to either an average element or to the peak-axial temperature in an average element and not to the over-all peak temperature anywhere in the core, which could be higher than the values given here.

Step Reactivity Insertions

Figure 34 shows the temperature distribution as a function of time following a 0.005 δk/k step reactivity increase with no scram action. It is seen that for such an accident severe cladding damage would result in approximately 4 seconds.

Figure 35 shows the average fuel-element and helium-outlet temperatures versus time following a 0.010 δk step increase in reactivity both with and without a 120-percent-power scram action. In this accident a scram action causes the average fuel-element temperature to peak at about 2120°F, but, owing to the axial local/average power distribution, the hot-spot cladding temperature (which is not shown on the figure) reaches a peak value of 3160°F 0.13 seconds before it starts to level off.

The assumption of step reactivity insertions without any scram action is so pessimistic and improbable that it was decided to determine the magnitude of step change that could be tolerated in EBOR, assuming in all cases that the core was scrammed after reaching 120 percent power and following a 40-millisecond delay time. These results are summarized in Figure 36, where the maximum values of the indicated temperatures reached at some time following the step change are plotted as a function of the δk/k of the step.

For these assumed accidents, the limiting temperature of the core is always the cladding. It is seen from Figure 36 that the maximum step change that can be controlled by the scram system is about 0.009 δk/k. Step increases greater than this make the core too prompt critical and, owing to the small heat capacity of the fuel pins and the short neutron-generation time, severe damage occurs immediately.

The effects of the temperature coefficient and a scram on the power following a 0.01 δk/k step reactivity insertion are shown in Figure 37, where the core power (in megawatts) is plotted against time. The dashed curve assumes no scram and the power reaches a peak value of about 16,500 megawatts at 0.05 second before being turned downward by the temperature

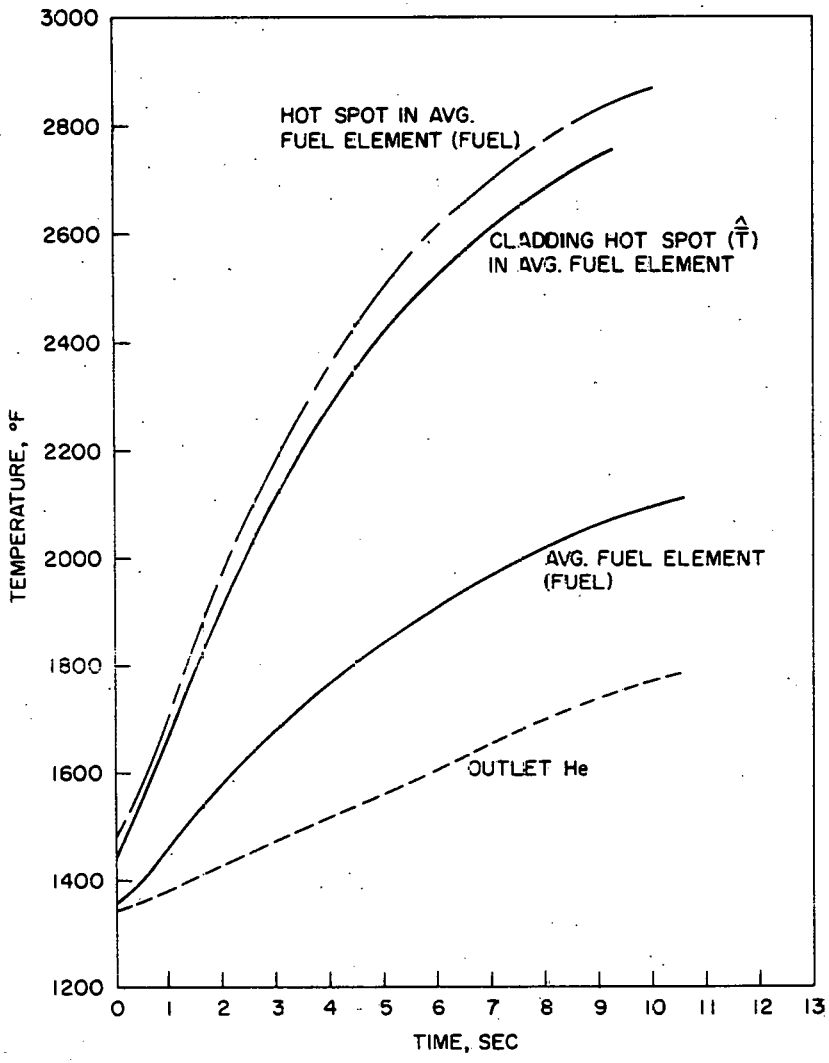

Fig. 34--Temperature versus time after a step δk change of 0.005; no scram

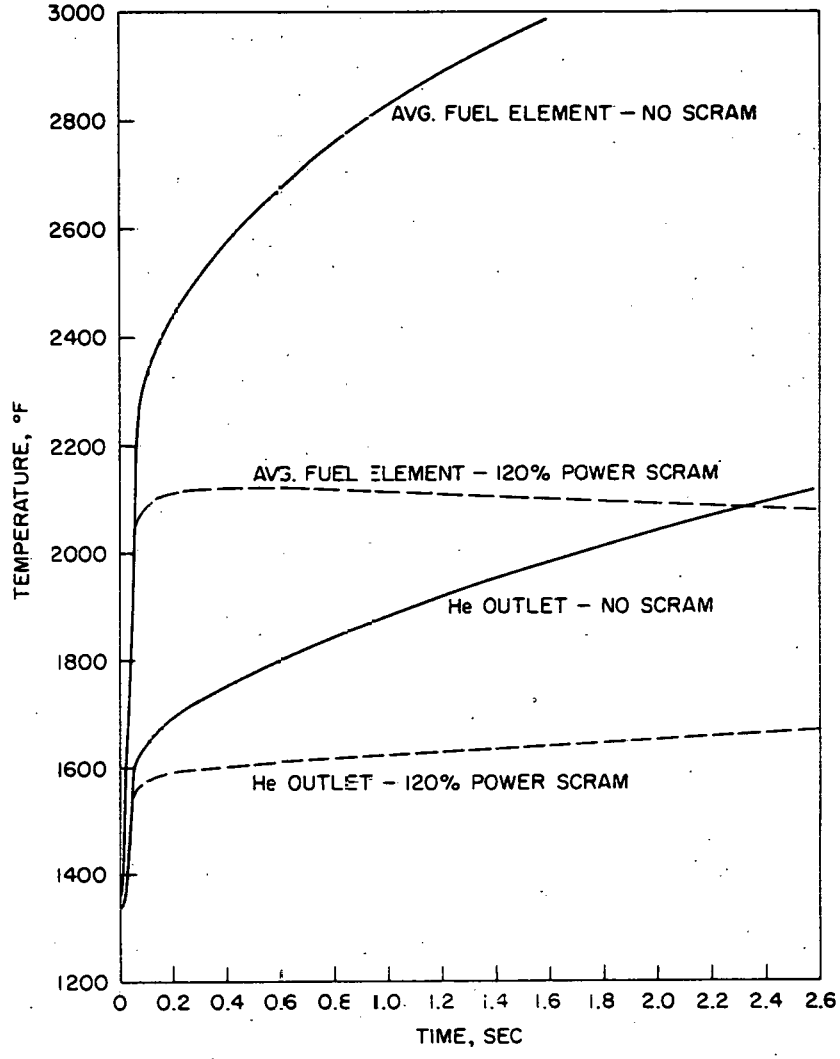

Fig. 35--Temperature versus time after a step δk change of 0.010

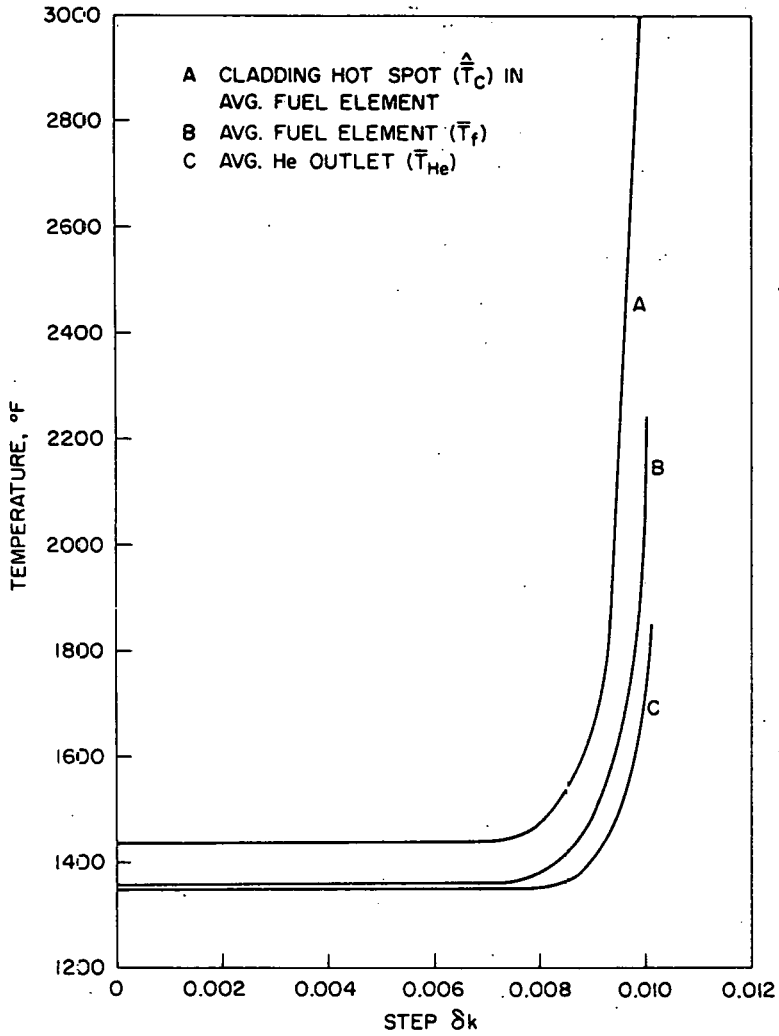

Fig. 36--Maximum temperature reached versus step δk for a scram at 120 percent power following a 0.040-sec delay

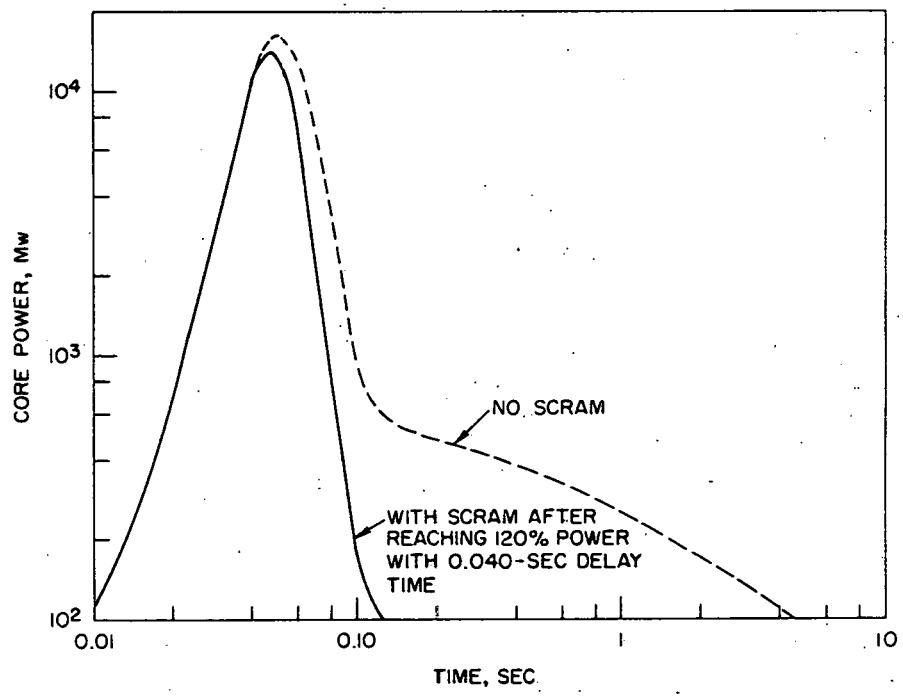

Fig. 37--Power versus time following a 0.01 δk step change

coefficient. The solid curve, which is for a scram at 120 percent power (12 Mw), peaks at about 14,000 megawatts and then drops rapidly.

Ramp Insertions of Reactivity

Calculations were also performed for several assumed ramp reactivity-insertion rates. EBOR rod-worth analyses predict the hot, clean rod-bank-insertion depth to be about 42 inches into the active core. In this analysis, it was assumed that a ramp accident occurs when one rod starts to withdraw at a rate of 2 inches/minute. The consequences of such an accident have been evaluated as a function of the insertion depth of the rod at the start of withdrawal. In all cases studied to date, no scram action was assumed.

In Figures 38 and 39, the temperatures and the reactivity contributed by the accident and the temperature coefficient are plotted against time for ramp insertions assumed to have started at 40-inch and 50-inch insertion depths, respectively. Owing to the strong variation in the differential rod worth as a function of insertion depth, the ramp reactivity rate is approximately two times greater at 50 inches rod insertion than it is at 40 inches. As a result, the rate of temperature rise is approximately twice as great for the 50-inch insertion.

The accident reactivity and the temperature-coefficient-reactivity feedback are plotted as a function of time in Figures 38 and 39. Also shown is the net reactivity, which is always very slightly positive for these cases; i. e., the temperature coefficient never quite cancels out the reactivity being added by the rod withdrawal.

The rate of temperature change in the average helium-outlet temperature and in the cladding hot-spot temperature in the average fuel element is plotted as a function of the assumed rod-insertion depth at the start of the ramp in Figure 40. It is seen from Figure 40 that at the calculated hot, clean rod-bank position of 42 inches, the withdrawal of one rod will cause the cladding hot-spot temperature to increase at the rate of approximately 210 $^{\circ}$F/minute. At this rate, some of the cladding in the average fuel element would reach melting temperatures in approximately 4-1/2 minutes.

Loss-of-coolant Flow

For the loss-of-coolant-flow study, it was assumed that the helium coolant flow was instantaneously lost and that no scram action was taken. In Figure 41, the pertinent temperatures and reactor power are plotted as a function of time. In the analysis of this case, it was assumed that the coolant failure occurred at 5 seconds for the time scale shown in the figure.

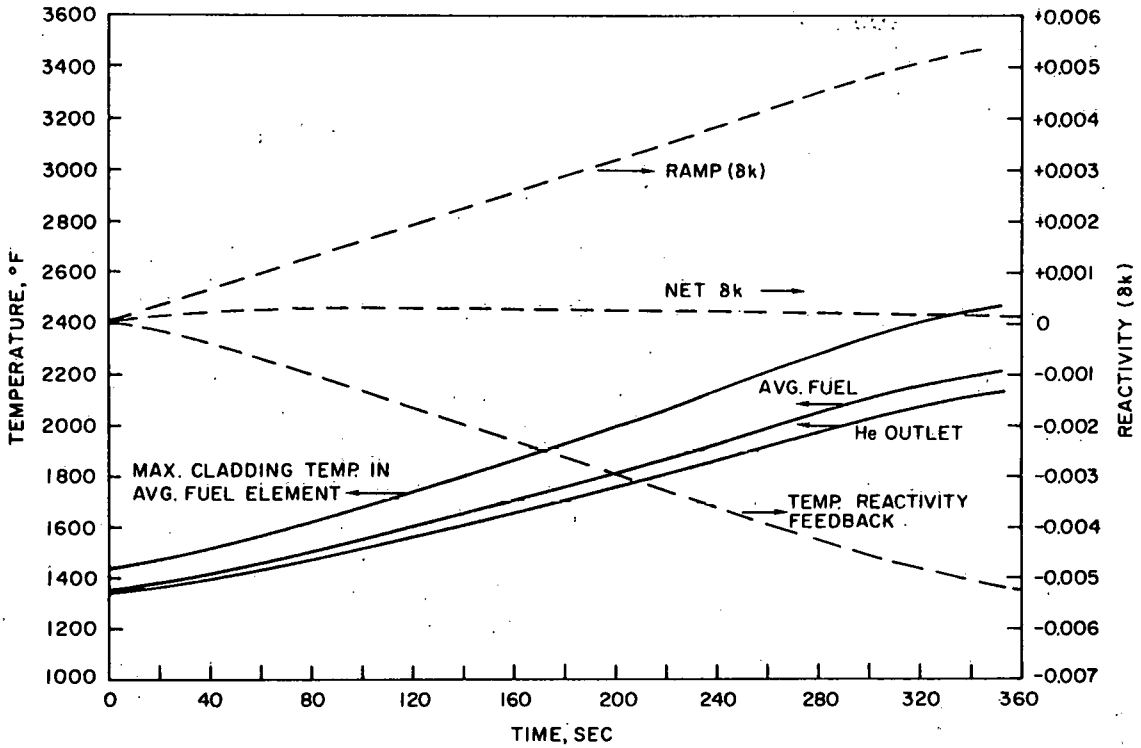

Fig. 38--Temperature and reactivity versus time for one rod withdrawal from 40-inch insertion depth; no scram

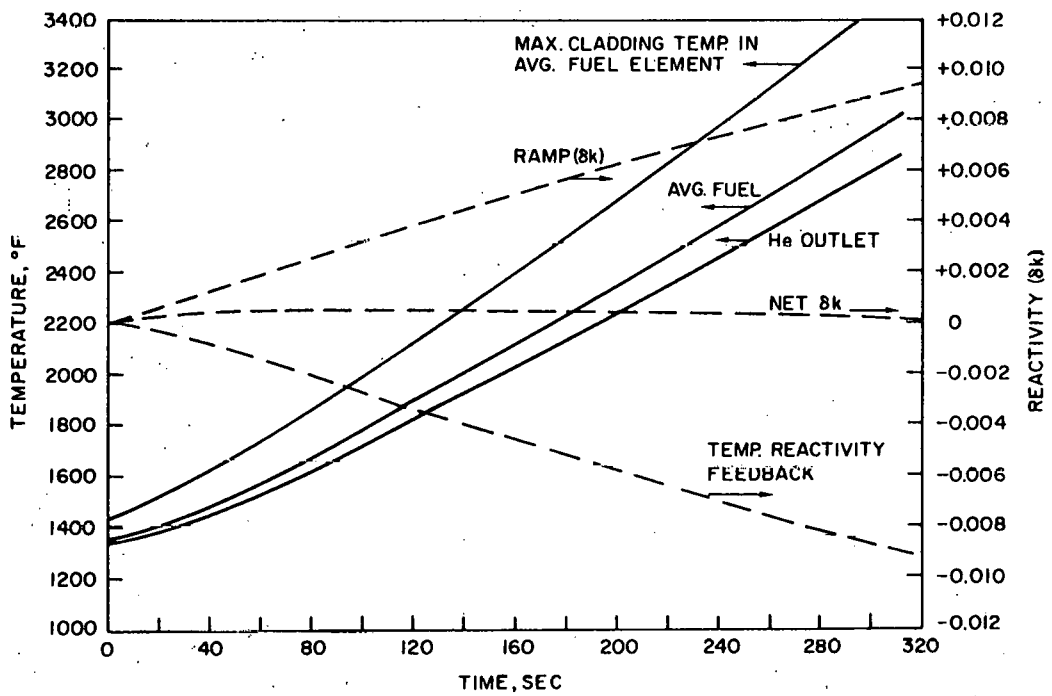

Fig. 39--Temperature and reactivity versus time for one rod withdrawal from 50-inch insertion depth; no scram

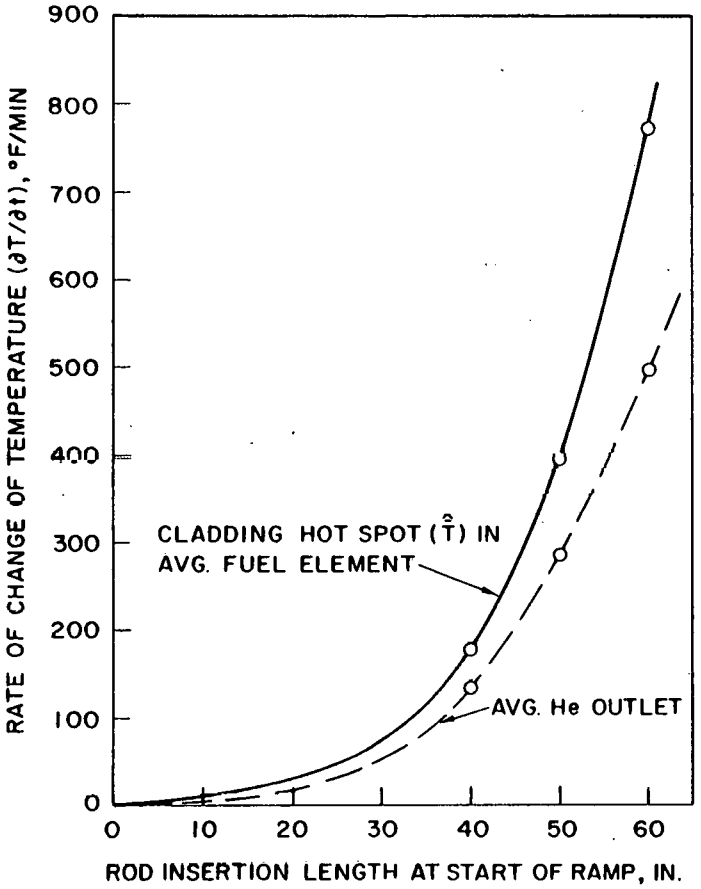

Fig. 40--Rate of change in temperature versus rod insertion length at beginning of ramp

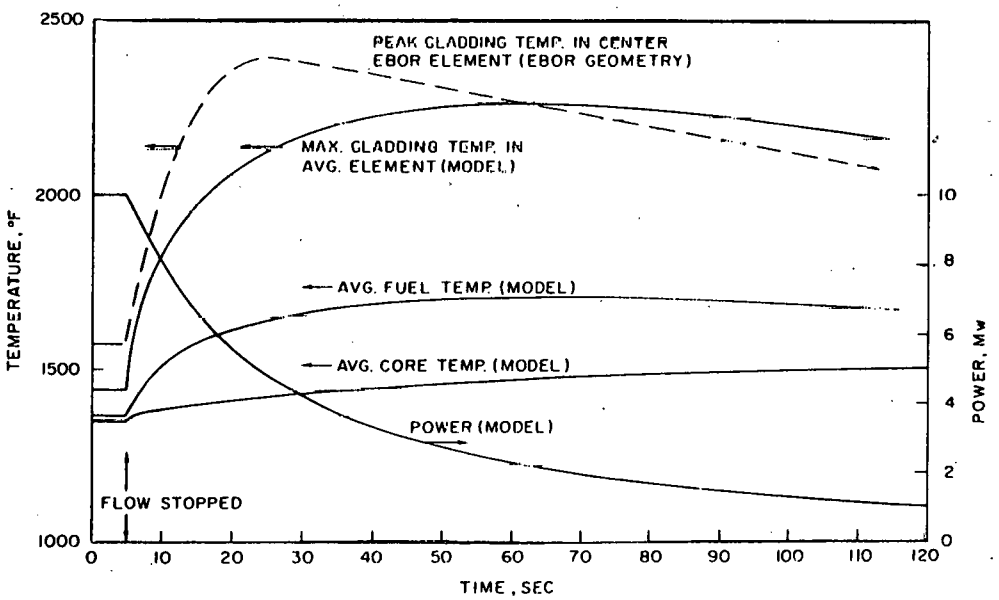

Fig. 41--Temperature and power versus time for loss of coolant; no scram

In the event of coolant loss and no scram, some asymptotic value of the average core temperature and the reactor power should eventually be reached owing to the feedback from the negative temperature coefficient. From Figure 41 it is seen that the asymptotic values have almost been reached after about 2 minutes. It is also of interest that the average fuel temperature passes through a maximum and then starts to decrease as heat from the fuel region is transferred to the moderator.

It should be pointed out that the model used in these studies underpredicts the rate of heat transfer from the fuel to the moderator and consequently is less valid for the loss-of-coolant analysis than for the other cases considered. This is because the model was set up to give the correct temperature in the fuel element and as nearly as possible the correct heat transfer to the coolant gas. However, for total coolant loss no heat is transferred to a gas and, consequently, the rate of heat transfer across the gap to the moderator determines the temperature reached in the fuel element and the cladding. Owing to the geometrical difference between the actual EBOR element and the model, the heat-transfer rate to the moderator is different for the two. This is primarily due to the fact that the actual surface area for heat transfer to the moderator in an EBOR element is about twice the area in the model geometry. In the analysis of this case, the gas conductivity was increased by a factor of two over the nominal value for helium to compensate for the differences in the heat-transfer area between the model and an EBOR element.

Fortunately, it is possible to compare the results of this calculation with results calculated from an EBOR heat-transfer code that handles the EBOR geometry explicitly. In this heat-transfer calculation, the reactor power as a function of time obtained from the above model calculation was used as input, since the explicit calculation is not a combined heat-transfer and kinetics calculation. The calculated temperature as a function of time obtained from the explicit calculation is shown in Figure 41 as a dashed curve. This is the temperature of the cladding at the point of peak heat-generation rate in the central EBOR element. This, then, corresponds to the hottest cladding temperature in the core, and the heat-generation rate corresponding to this point was about 26 percent higher than the heat-generation rate at the point of maximum cladding temperature for the average element that was calculated with the model geometry.

A comparison of the two cladding temperatures, given in Figure 41, shows that the model calculation probably gives a good indication of the peak temperatures reached following the loss of coolant. However, as expected, the model underpredicts the heat-transfer rate from the fuel to the moderator and consequently predicts that the fuel and cladding temperatures will remain at elevated temperatures longer than is actually the case.

REFERENCES

1. Goodjohn, A. J., and A. D. Mc Whirter, "Temperature Coefficient Calculations for the Experimental Beryllium Oxide Reactor," General Atomic Report GA-4130, May, 1963.

2. Keepin, G. R., T. F. Wimett, and R. K. Zeigler, "Delayed Neutrons from Fissionable Isotopes of Uranium, Plutonium, and Thorium," Phys. Rev., Vol. 107, 1957, p. 1044.

IV. MATERIALS DEVELOPMENT

FUEL MATERIALS

Irradiation of Fuel Materials

Performance studies of fuel materials for the EBOR under conditions of high-temperature irradiation were continued during this quarter.

Capsule MGCR-4

The MGCR-4 capsule experiment was designed to study the effect of fuel-particle size on the performance of 70 BeO–30 UO_2 (volume percent) fuel pellets at temperatures and heat-flux conditions that are of interest in the EBOR program. The fuel pellets for the capsule were fabricated at General Atomic and contained 30 volume percent UO_2 dispersed in a BeO matrix as fine (approximately 10-micron-diameter) particles in half of the pellets and as coarse (approximately 150-micron-diameter) particles in the remaining pellets.

The capsule was inserted in a reflector position in the MTR on June 16, 1961, and was discharged from the reactor on March 11, 1963, having accumulated 11,700 hours of irradiation at full power encompassing 170 cycles. This corresponds to an estimated peak burnup of 4.8 percent of the uranium atoms present (approximately 3.6×10^{20} fissions/cm^3; 42,000 Mwd/ton of uranium).

The Monel cladding on seven of the eight specimen pins was severely cracked. This precluded fission-gas-release analysis for these seven; a gas sample from the eighth pin was collected and is undergoing analysis.

All 16 samples of seeded fuel (100- to 150-μ UO_2 particles) were removed from their pins as whole pellets. All 16 samples of the homogeneous fuel (0- to 25-μ UO_2 particles) were broken; 13 were badly fragmented, three of which were in large pieces. The diameter and length of all of the seeded fuel pellets increased 0.5 to 1 percent. Density measurements will be used to infer dimensional changes that might have occurred in the homogeneous fuel pellets.

Items of the postoperation examination and analysis still awaiting completion include fission-gas-release analysis, uranium-burnup calculations, isotope burnup, fission-product analysis, meltdown tests to

augment fission-gas-release data, metallography, and determination of postirradiation strength.

Eight specimens from the temperature-history mockup of the MGCR-4 fuel capsule were submitted for measurement of fission-gas release after tracer-level irradiation. Surface-area measurements were made on the samples, but fission-gas-release analysis has not been completed.

Capsule MGCR-BRR-9

The MGCR-BRR-9 fuel capsule was designed and fabricated at Battelle Memorial Institute and irradiated in the MTR for 18 reactor cycles. The capsule contained BeO–UO_2 fuel pellets identical to those irradiated in the MGCR-4 capsule. The capsule was discharged from the reactor on November 19, 1962, after experiencing a burnup, as indicated by dosimetry analysis, of 3.34 percent of the uranium atoms present (approximately 2.2×10^{20} fissions/cm^3; 28,800 Mwd/ton of uranium).

As reported in the previous quarterly report (GA-4124), all of the fuel pellets in the capsule had cracked, precluding a direct determination of dimensional change. The results of density determinations are listed in Table 5; from these results it has been determined that the linear increase in length and diameter was approximately 1.5 percent. No differences were found between measurements of the fine-particle and the coarse-particle fuel pellets.

Table 5

DENSITY OF FUEL SPECIMENS FROM MGCR-BRR-9 CAPSULE

Pellet No.	Preirradiation Bulk Density		Postirradiation Bulk Density		Change in Density, %
	g/cm^3	% Theo.	g/cm^3	% Theo.	
F-106	5.16	95.6	4.93	91.3	-4.5
F-107	5.12	94.8	5.00	92.6	-2.3
F-108	5.21	96.5	5.03	93.1	-3.5
F-109	5.02	93.0	----	----	----
F-110	5.18	95.9	----	----	----
F-111	5.13	95.0	----	----	----
C-124	5.05	93.5	4.80	88.9	-4.5
C-125	5.02	93.0	----	----	----
C-126	5.04	93.3	4.91	90.8	-2.4
C-127	5.03	93.1	----	----	----
C-128	5.06	93.7	----	----	----
C-129	5.02	93.0	----	----	----

Fission-gas-release measurements, made by puncturing the individual fuel pins in the hot cell, indicated that the coarse-particle fuel pellets released approximately 20 percent of the krypton during irradiation and the fine-particle fuel pellets released less than 1 percent (see Table 6). This behavior is just the inverse of that predicted theoretically and that previously observed by other experimenters who have investigated fine- and coarse-particle fuel-dispersion materials under different irradiation conditions. The reason for this behavior is presently unknown. Fuel-meltdown tests are under way on these irradiated fuel samples to confirm the above results.

Table 6

FRACTIONAL RELEASE OF KRYPTON-85

Specimen No.	Fuel-particle Size	Fission Density, f/cm^3	Total Fissions	Kr^{85} Atoms Formed	Fraction Released
4	Fine	2.01×10^{20}	3.95×10^{20}	1.16×10^{18}	ND[a]
1	Fine	2.19×10^{20}	4.35×10^{20}	1.27×10^{18}	ND[a]
3	Coarse	2.28×10^{20}	4.42×10^{20}	1.30×10^{18}	0.242
6	Coarse	2.28×10^{20}	4.40×10^{20}	1.29×10^{18}	0.176
2	Fine	2.07×10^{20}	4.08×10^{20}	1.20×10^{18}	0.003
5	Coarse	2.01×10^{20}	3.90×10^{20}	1.14×10^{18}	0.232

[a]None detected.

Work remaining on the examination of the MGCR-BRR-9 capsule includes isotope and fission-product determination of burnup and meltdown studies.

REACTOR MATERIALS

Moderator Materials

Studies of the effects of irradiation on the behavior of BeO-moderator ceramics were continued during the quarter.

Capsule MGCR-2

The MGCR-2 capsule, containing 134 beryllium oxide specimens embodying three different compositions, was irradiated in the GETR, was terminated prematurely on January 5, 1963, and was examined in the

General Atomic hot cell. Calculation of data from flux-wire dosimeters indicate that the average exposure for the capsule was 1.0×10^{21} nvt (>1.0 Mev) at an average flux of 1.17×10^{14} nv. Temperature distribution in the capsule is being determined.

Measurements of dimensions and densities of the irradiated BeO specimens, completed during the quarter, are listed in Table 7. The physical appearance of all of the samples containing bentonite was good except for diametral cracks in the 1.68-inch-diameter pieces from the hotter portion of the capsule. It is believed that the diametral cracks resulted from the difference in thickness expansion as a function of radius. This difference would result in tensile stresses being generated at the center of the pellet. This interpretation is supported by the existence of occasional cracks extending from the central portion of the pellets toward the outside surface.

Table 7

PERCENTAGE CHANGE IN DENSITY AND DIMENSION OF BeO FROM MGCR-2 CAPSULE

Capsule Position	Theoretical-density Change, %	Linear-dimension Change, %		
			Thickness	
		Diameter	Outer Edge	Center
Cooler end	-1.6 to -2.5	0.44 to 0.82	0.50 to 0.72	0.10 to 0.56
Hotter end	-3.0 to -3.7	1.18 to 1.44	0.96 to 1.38	0.34 to 1.22

A preliminary evaluation of the room-temperature thermal-conductivity changes for the specimens containing bentonite, based on thermal-diffusivity measurements, indicates that the conductivity of pieces irradiated in the cooler end of the capsule retained approximately 20 percent of the original value and pieces irradiated in the hotter portion of the capsule retained approximately 25 percent of the original thermal conductivity. Modification of the thermal-diffusivity apparatus, to permit measurements at elevated temperatures, is complete and thermal-diffusivity measurements over a range of temperatures will be initiated during the next quarter.

A much larger proportion of the specimens containing 1 percent MgO or 0.5 percent MgO plus 0.5 percent Al_2O_3 was found to be broken. This was particularly true for the 1.68-inch-diameter rings, of which only 9 of the 24 examined remained intact; only one of these intact rings was a low-density specimen. Of the 24 inner rings examined, 10 were broken, 9 of

which were low-density specimens. Of the 24 plugs examined, 4 were broken, all of which were of low density. Two of the high-density outer rings containing large-size grain and 1 percent MgO flux had disintegrated to powder except for two or three fragments.

Diametral increases for the 24 plug specimens ranged from 0.28 to 1.41 percent, and the thickness changes varied from minus 0.48 to plus 1.16 percent. Corresponding density changes ranged from 0.3 to 6.0 percent decrease.

Cylindrical specimens, 0.3 inch in diameter, are being core-drilled from both preirradiation and postirradiation samples to evaluate both the strength and thermal diffusivity.

BeO Irradiation in MGCR-4

In addition to the fuel pellets contained in the MGCR-4 fuel-irradiation capsule, 16 beryllia samples were also irradiated in the capsule as part of the BeO irradiation study. The samples consisted of pellets prepared from UOX-grade BeO containing 1 weight percent MgO. Measurement of the samples after irradiation indicated that there was no detectable change in the diameters. The diameters of the beryllia pellets were determined to within 0.001 inch, which corresponds to an accuracy of 0.25 percent. The fast-neutron flux to which the specimens were exposed is being determined by analysis of dosimetry data.

BeO Development

Work to determine whether a fatigue mechanism will influence the modulus-of-rupture strength of BeO materials continued during the quarter.

The specimens used in the tests were machined from unirradiated BeO blocks that were fabricated to the specifications for EBOR moderator blocks. Testing of the BeO bars is complete. Metallographic and electron-probe studies are continuing. Table 8 gives the significant data obtained during testing.

Results indicate that a fatigue mechanism will not cause failure of the BeO in the temperature range 1000° to 1600°F if the pieces are repeatedly subjected to a maximum stress of less than 85 percent of the anticipated uncycled modulus of rupture. In fact, the results indicate that a significant strengthening of the EBOR material may be gained after cycling to less than 85 percent of the anticipated uncycled modulus of rupture. An indication that a fatigue mechanism may be operative (not shown in Table 8) was observed for bars subjected to a maximum stress of greater than 85 percent of the anticipated uncycled modulus of rupture.

Table 8

MODULUS OF RUPTURE, STRESS CYCLE, AND YOUNG'S MODULUS FOR BeO AT VARIOUS TEMPERATURES

Temp. (°F)	Modulus of Rupture, psi		Stress-cycle Range, psi	Young's Modulus Before Cycling, psi
	Before Cycling	After 1000 Cycles		
1000	28,900	30,200	1 to 25×10^3	37.7×10^6
1300	35,100	34,400	1 to 25×10^3	37.4×10^6
1400	31,400	----	----	34.8
1450	23,300	----	----	35.6×10^6
1500	18,700	----	----	34.9×10^6
1600	14,600	15,600	1 to 12.3×10^3	27.2×10^6
1700	14,150	----	----	28.6×10^6
1800	9,990	----	----	27.9×10^6

The mean uncycled modulus-of-rupture values for the EBOR BeO moderator in the temperature range 1000° to 1800°F were substantially lower than the values for UOX-grade BeO reported in the literature. The abrupt decrease in uncycled modulus of rupture at approximately 1400° to 1450°F can possibly be attributed to the softening of an intergranular glassy phase.

The measured, uncycled, Young's-modulus values in the observed temperature interval were substantially lower than values for AOX-grade BeO reported in the literature. A distinct decrease in uncycled modulus values was observed at approximately 1500°F.

A correlation of uncycled modulus-of-rupture values for bars from four corresponding blocks indicated that two blocks were relatively weak and two were strong.

Control-materials Development

The objective of this task is to develop control-rod materials for use in the EBOR program.

Capsule MGCR-7

The MGCR-7 absorber-materials capsule was designed for the irradiation of Al_2O_3–Dy_2O_3 absorber materials with a range of compositions of interest for EBOR applications. The capsule was installed in the ETR and irradiation began November 9, 1962. An exposure equivalent to 2350 hours at reactor full power was attained during irradiation through May 26, 1963.

Evaluation of the out-of-pile reference specimens for the irradiation experiment was completed during the quarter, with the exception of high-temperature thermal-diffusivity measurements. A summary of significant results obtained at room temperature is shown in Table 9. Tensile-strength values for materials representative of those being irradiated were determined by the diametral-compression-test method. High-temperature thermal-diffusivity measurements are scheduled for the next quarter.

Table 9

TENSILE STRENGTH AND YOUNG'S MODULUS FOR EBOR ABSORBER MATERIALS

Group	Dy_2O_3, wt-%	Density, g/cm^3	Tensile Strength, psi	Young's Modulus, psi
1	4.7	3.467	17,720	$\sim 25 \times 10^6$
2	26.6	4.494	24,220	$\sim 53 \times 10^6$
3	46.7	4.926	15,020	$\sim 43 \times 10^6$
4	67.2	5.450	10,080	$\sim 34 \times 10^6$

V. CONSTRUCTION ENGINEERING

Completion of Title II design was reported in the previous quarterly report (GA-4124). During the present quarter the AEC office in Washington, D. C., granted release for construction, and the AEC Idaho Operations Office released the plans and specifications to the construction contractor on June 5, 1963.

Purchase orders for all major pieces of equipment to be purchased by General Atomic have been placed. Many pieces of equipment have been obtained and are now in storage at the National Reactor Testing Station (NRTS).

As mentioned in previous reports, the EBOR will be constructed at the site of the former Shield Test Pool Facility, which was part of the General Electric/Aircraft Nuclear Propulsion Department complex, situated at the north end of NRTS. This area has since been designated as Test Area North (TAN). Figure 42 shows the location of the facility and the shaded areas of Figure 43 define the modifications and additions planned to adapt the facility for the EBOR installation.

The facility as it now exists includes two pools, each of which measures 25 feet wide, 40 feet long, and 30 feet deep. The south pool will be divided into two sections: the south section will house the reactor and the north section will contain the pressure-vessel-head storage area. The south section will be deepened by approximately 20 ft to accommodate the reactor. The concentric duct will exit south from the reactor through a tunnel about 23 feet below grade level. The regenerator will be situated at the end of the concentric duct. The helium piping leading to and away from the regenerator will pass through a tunnel normal to the tunnel that houses the concentric duct and will rise to the machinery vault at grade level.

The machinery vault contains the main helium circulator, decay-heat-removal blower, and the emergency air compressor, which will cool the reactor core in the event of a loss-of-coolant accident.

The helium-to-air heat exchanger will be located in a plenum below the stack, which is 150 feet high and 8.5 feet in diameter at the top. In the unlikely event of a helium leak in the heat exchanger, contaminated helium will be dispelled through the stack. The building ventilation system is

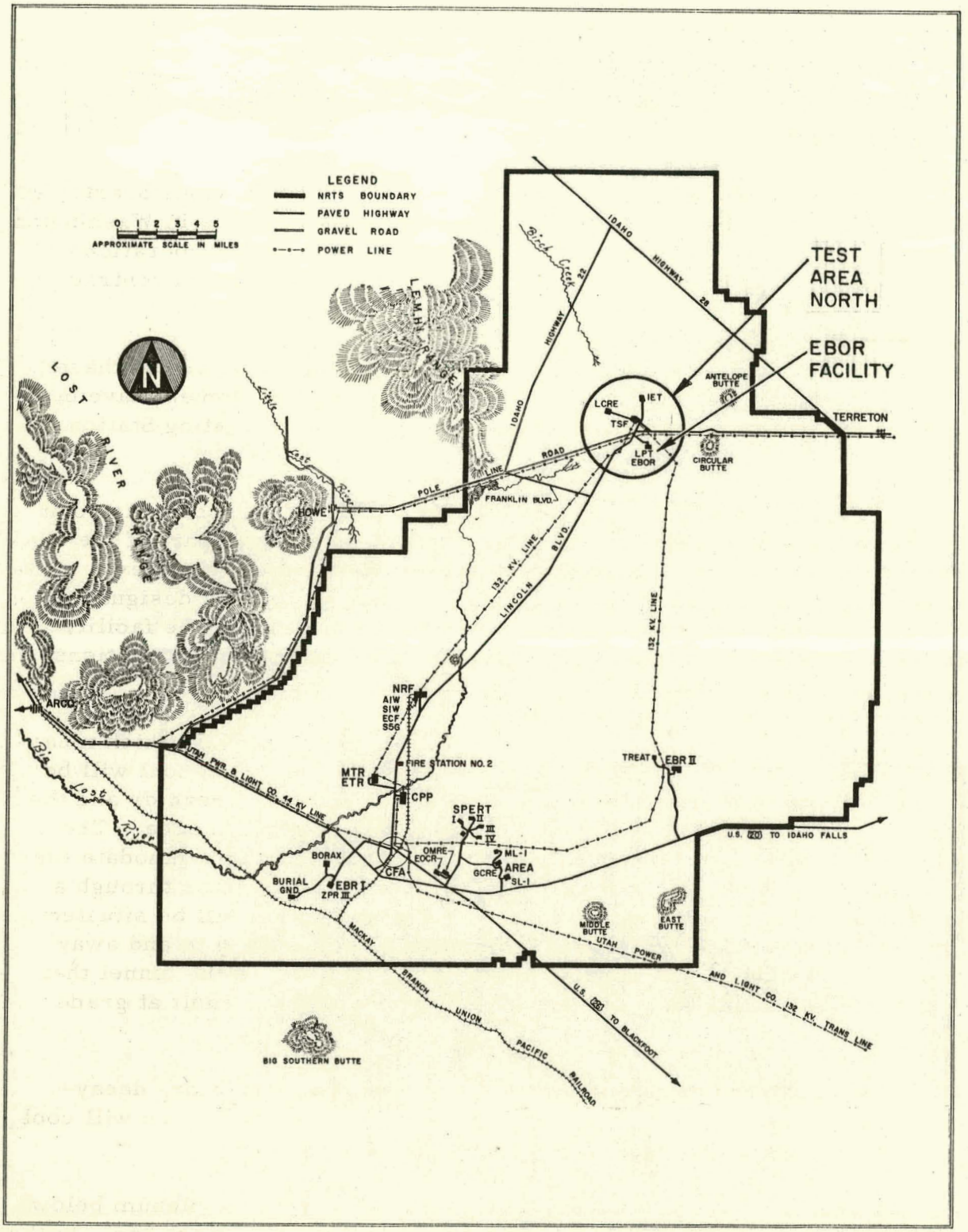

Fig. 42--Map of National Reactor Testing Station showing Test Area North

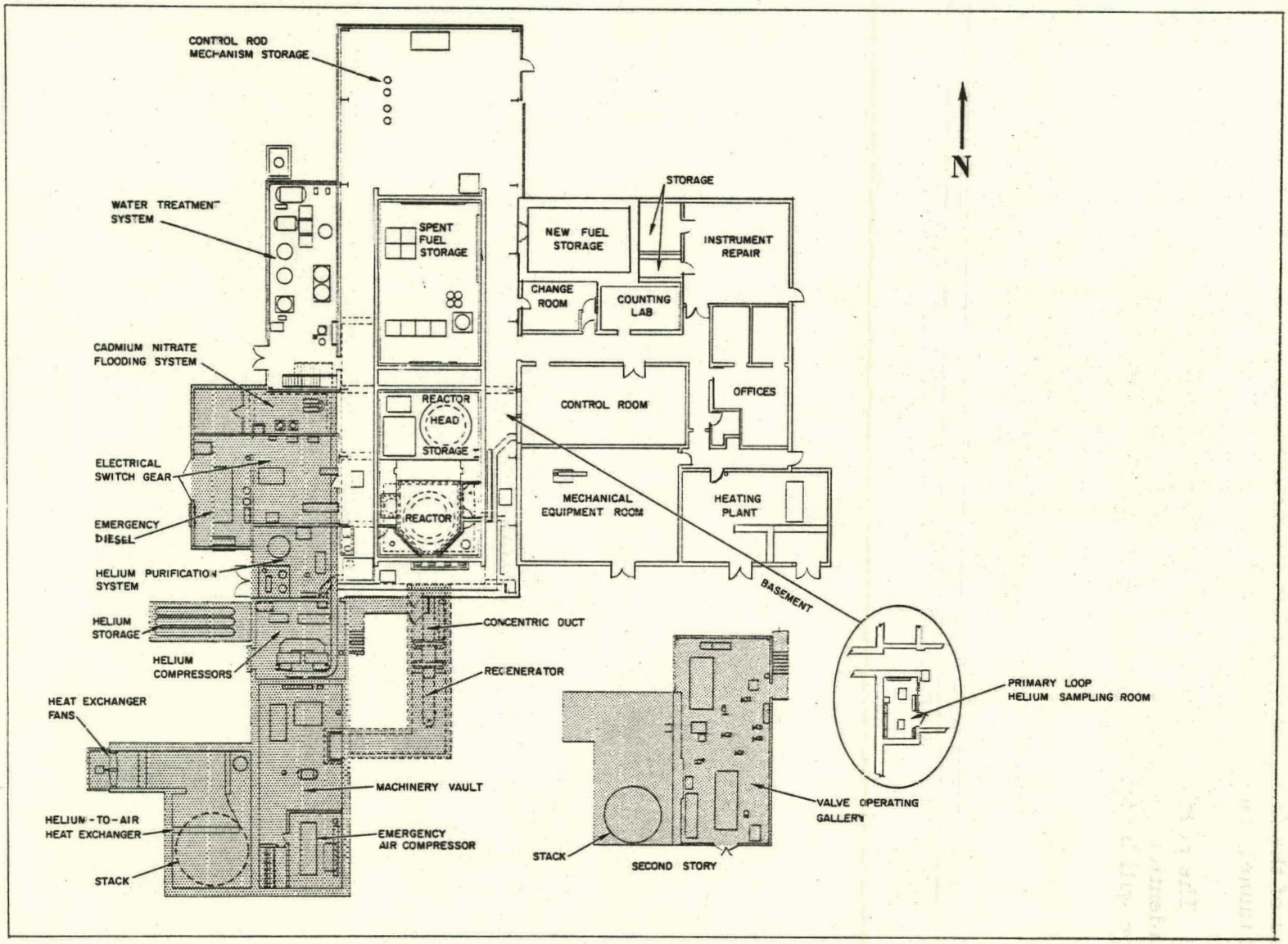

Fig. 43--Layout of Shield Test Facility showing modifications for adaptation to EBOR test facility

designed as a once-through system. Air is supplied first to the inhabited areas of the facility, then is exhausted through the reactor vault, concentric-duct tunnel, and machinery vault and out through the stack.

The north pool in the building will remain unchanged; its dimensions are identical to those of the south pool. Its function in the over-all installation will be for the storage of spent fuel.